Soil Biology and Biochemistry 194 (2024) 109417

Contents lists available at ScienceDirect

Soil Biology and Biochemistry

journal homepage: www.elsevier.com/locate/soilbio

Microdialysis probes and digital twins reveal the rapid removal of fertiliser phosphate from the soil solution with an impact on crop nutrition in the short-term

C. Petroselli [a,b,1], K.A. Williams [a,c,1], S.A. Ruiz [a,1], D. McKay Fletcher [a,e,1], M.J. Cooper [d], T. Roose [a,*]

[a] University of Southampton, School of Engineering, Faculty of Engineering and Physical Sciences, Southampton, UK
[b] University of Perugia, Department of Chemistry, Biology and Biotechnology, Perugia, Italy
[c] University of Portsmouth, Faculty of Science and Health, Portsmouth, UK
[d] University of Southampton, National Oceanography Centre, Southampton, UK
[e] Scotlands Rural College, Rural Economy, Environment and Society Research Group, Edinburgh, UK

ARTICLE INFO

Keywords:
Phosphorus
Microdialysis
X-ray computed tomography
Image-based modelling
Precision agriculture

ABSTRACT

Global food production depends on the application of phosphorus (P) fertilisers, usually sourced from rock phosphate, a non-renewable resource. Optimising P use to ensure sustainable P application is necessary to supply food worldwide and to protect the environment from P runoff. However, standard models used to guide P application on fields are limited due to assumptions that fail to consider the short-term dynamics of P in the soil solution. This study combined time-resolved microdialysis sampling with 4D spatial information from X-ray computed tomography to inform an image-based model for assessing P-soil-plant interactions over the start of a growing season. The time-resolved microdialysis measurements revealed that P released from the granules is rapidly removed from the soil solution in the short-term. We demonstrate that the standard equilibrium models typically used to characterise P transport in soil are not representative of the experimental system on the time scales considered. Instead, an Absorption-Diffusion model, where a single sink term accounts for all the processes removing P from the soil solution was required to correctly characterise experimental observations. Our study provides the basis for a model which could be adapted to predict within-season fertilisation scenarios in different soil conditions, and provides a conceptual description of plant/crop yield response to P fertilisation.

1. Introduction

Phosphorus (P) is an essential plant nutrient, and one that is often yield-limiting in agricultural systems. Thus, P availability to crop plants is vital for productive agriculture and efficient land use (Barber, 1995). Global demand for P fertiliser has increased with growing human population (Cordell et al., 2009) and P-fertiliser prices increased from 120 to 320 EUR per metric ton in the last year (2022 (Mundi, 2022);). Soil P stocks and access to P fertilisers are not equally distributed around the world. One in five children worldwide are affected by malnourishment linked to fertiliser (*i.e.* P) scarcity (Kahiluoto et al., 2021), but in much of Western Europe, the USA and China, agricultural soils show high total P content due to over fertilisation in 20th century (also called legacy P). Phosphorus accumulation in the EU and the US soils ranges from 700 to 800 kg ha^{-1} and 230–1400 kg ha^{-1}, respectively (Kahiluoto et al., 2021). In some cases, ceasing the application of P fertiliser would not have an adverse effect on yield for several years (Valkama et al., 2011; Sattari et al., 2012, 2014). In developed nations, farmers are hypothesised to keep the soil P levels high as insurance against P deficiency limiting yields and to use the soil as a 'bank' to protect against increases in future P fertiliser prices (Macintosh et al., 2019). However, in sub-Saharan Africa and less developed sub-tropical country agricultural soils, insufficient P input limits yields (Nziguheba et al., 2016). Phosphorus deficits in developing countries are on the order of 125–250 kg

* Corresponding author. School of Engineering, Faculty of Engineering and Physical Sciences, University of Southampton, University Road, Southampton, SO17 1BJ, UK.
E-mail address: t.roose@soton.ac (T. Roose).
[1] Denotes equal contribution by authors.

https://doi.org/10.1016/j.soilbio.2024.109417
Received 30 October 2023; Received in revised form 19 March 2024; Accepted 26 March 2024
Available online 5 April 2024

ha^{-1} affecting ~200–300 Mha of arable land area (Kahiluoto et al., 2021).

Together, the over application of P in some regions, depletion of P in others, and a looming P supply crisis require efforts to optimise P use efficiency on the global scale, on the scale of individual fields and even on individual fertiliser granule scale. One approach to tackling P use efficiency is to optimise the within-season use of P fertiliser using precision agriculture approaches (Cisternas et al., 2020; Ros et al., 2020); this requires an understanding of the fundamental processes underlying short timescale P dynamics and uptake in soil. Low Soil Test Phosphorus (low-STP) soils typically have a larger yield response to P fertilisation than high-STP soils (Ros et al., 2020). However, it remains unclear as to when farmers can expect larger yield responses. Some of these uncertainties can be attributed to theoretical assumptions based on long term observations that may not be valid in low-STP soils at shorter timescales.

Phosphorus fertilisation usually includes the application of P as soluble compounds that release phosphate into the soil solution where plant roots can directly access it (Hedley and McLaughlin, 2005). The application of P soluble compounds generates a sharp increase in P soil solution concentration, which favours the plant uptake, but could also result in P leaching and runoff leading to pollution and eutrophication of water bodies (Cornish, 2009). It is well known that most of the supplied P (about 70%) is not taken up by plants in the first harvest, but it is retained in the soil (Barrow, 1980) and is thought to keep sustaining the crops as a long-term P-legacy, even though its efficiency greatly decreases over time (Bolland and Gilkes, 1998). However, the understanding of intra-seasonal short-term dynamics of P in the soil solution, that could shed light on how to maximize the effect of the supplied P on crops while reducing runoff, is less well understood as high frequency time-resolved techniques are (Demand et al., 2017; Gao et al., 2019a; Petroselli et al., 2021). Phosphorus concentration in the soil solution decreases after fertiliser application mainly due to sorption, i.e., adsorption onto soil particles surfaces followed by possible absorption inside the soil solids structure (Barrow, 1983) and precipitation of secondary P-rich phases driven by oversaturation or favoured by sorption (Pierzynski et al., 2005). Moreover, microbially mediated immobilisation (i.e. conversion of inorganic P into organic P) and the opposite process, mineralisation, also have an important effect in the P cycle in natural soils (Condron et al., 2005). In this paper, we are going to refer to retained-P as the fraction of P that is removed from the soil solution due to the combined effect of all the aforementioned processes, i.e., the P that is not immediately available to plants in soil solution. Typically, the proportion of retained-P to solution-P is between 40 and 1000 (Barber, 1995) and the concentration of P in the soil solution is < 10 μM (Schachtman et al., 1998). Therefore, the availability of P to plants depends on how quickly P is removed from the soil solution due to sorption, precipitation, immobilisation and microbial uptake. While certain mathematical models consider explicit reactions and rates of binding (Barrow, 1974), they are often limited to bulk estimation of parameter values that do not resolve spatial or even temporal small scale distributions of P. The typical theoretical model invoked to resolve transport of P and spatial distributions in soil relies on equilibrium reaction assumptions. In particular, the ratio between solution-P and retained-P is considered to be immediately in equilibrium based on the assumption that these reactions occur at rates more rapid than the rates of transport through soil (*i.e.* diffusion) (Barber, 1995). Under this model assumption, the P repeatedly binds and dissolves again from the soil surface, which slows its net rate of transport, leading to effective slow diffusion of P through soil. While this model is appropriate for large field sites or ecosystems over long time scales to describe dynamics of legacy-P, it cannot account for short-term local processes. For example, a recent study demonstrated that in small scale experiments low soil test P soils acted as sinks for even relatively large fertiliser applications (Petroselli et al. (2021)). Quantities of P fertiliser in excess of those applied to farm fields were found to be rapidly removed from the soil solution and were not measured again in solution after a 2-week period. While the P sorption and desorption almost certainly reaches an equilibrium, in this study the measured desorption from the soil was negligible. Petroselli et al. (2021) also observed rapid transport of P up to distances of 3 cm from the fertiliser granule, which, while being coherent with previous observations (Benbi and Gilkes, 1987), is not reproduced by the standard equilibrium mathematical model, which predicts a significant impedance to diffusive fluxes. In other words, the assumptions of a standard equilibrium model are not compatible with experimental results at small time and space scales. These results highlight a limitation to the standard equilibrium reaction assumption on intra-seasonal plant scale processes and suggest the need for an alternative dynamic modelling approach for low-STP soils. This has implications for field-scale predictions, because if P exists in the soil solution only for a narrow period of time (as suggested by rapid removal from soil solution), the timing of fertiliser application with respect to weather patterns and crop demand is crucial to get the most yield from the concentrated soil solution. However, gaining sufficient understanding of the dynamics of P in the soil solution at high temporal and spatial resolution requires time- and space-resolved experimental measurements of P concentrations.

This spatiotemporal approach is challenging, however, state of the art micro-sampling techniques, including suction cups and microdialysis probes, are helping to elucidate the underpinning processes that mediate P-dynamics in soil. Although these probes were originally designed for pharmacokinetics (Hammarlund-Udenaes, 2017; Petroselli et al., 2021), they can be used to sample the soil solution *in situ* and gain time resolved data on soil solution concentrations (Gao et al., 2019b; Petroselli et al., 2021). Microdialysis probe solute measurements have been used less frequently, but they have an advantage over suction cups as the measurements rely on passive diffusion of P across a semi-permeable membrane thus not affecting soil water transport. Moreover, microdialysis probes mimic root solute uptake from the soil solution, and have therefore been used as artificial roots (McKay Fletcher et al., 2019; Buckley et al., 2020; König et al., 2022).

Time resolved *in situ* chemical sampling is a powerful technique in itself, but its coupling with time-resolved 3D imaging of exact experimental setups and plant root structures enables to develop an image-based, 3D, spatially and temporally explicit model, which can act as a digital twin of the experimental system. Previous studies have demonstrated the utility of X-ray computed tomography (XCT) imaging as a tool for assessing spatial trends associated with plant development under varying fertilisation treatments (Ahmed et al., 2016). For example, morphometric features in these imaging studies were able to assess that root system architecture was broader in soils without fertilisation *vs* those with fertiliser granules, indicating plants employ an 'exploration strategy' under low-STP conditions (Williams et al., 2022). Furthermore, the present study used the XCT images to generate mathematical models, which extended the utility of the imaging. The models were able to make predictions about soil solution P concentrations, transport, and root P acquisition (Williams et al., 2022). Using this information, the model was able to predict optimal fertilisation strategies based on P availability in the soil solution and general soil buffering.

The current study builds on the aforementioned results by combining time resolved microdialysis sampling, XCT measurements, and image based modelling. Specifically, the study.

- Develops an experimental set up considering growing wheat plants in pots under different fertilisation regimes (early, late, and no P fertilisation);
- Measures soil solution P dynamics using high frequency microdialysis sampling at varying depths along the pot;
- Monitors root system development using time lapsed XCT imaging for the different treatments;
- Assess the suitability of two different image-based modelling approaches for simulating the experimental results;

- Develops an inverse modelling protocol to match the model results to the microdialysis measurements.

Our aim is to quantify soil solution P dynamics in a low-STP soil, compare the efficiency of different fertilisation protocols with different timings relative to plant root growth, and test if the dynamics of plant available P can be replicated using two different models: The buffer power model which assumes that the soil-P reactions are in equilibrium resulting in impeded diffusion; and the Absorption-Diffusion model which considers the removal of solute (e.g. surface binding, aggregate trapped, microbial activity) from the soil solution to be the dominant reactive process governing P transport and root uptake.

2. Materials and methods

2.1. Experimental set up

The experimental setup was adapted from previous studies (Ahmed et al., 2016; Williams et al., 2022) that integrated microdialysis sampling into an assay suitable for X-ray Computed Tomography (CT). PVC tubes with an external diameter of 110 mm and a height of 450 mm were used as support for the soil columns. Sandy clay loam Eutric Cambisol soil from an agricultural grassland in the Henfaes Research Station in Abergwyngregyn, Wales (UK; 53°14′N, 4°01′W) was oven-dried at 70 °C overnight and sieved to pass 2 mm. Dry bulk density was $\rho_b = 1.26 \pm 0.01$ g mL^{-1}. The soil properties are reported in Supplementary Table S1. Olsen-P test results for this soil have been extensively reported in previous publications (Oburger et al., 2009, 2011; Ahmed et al., 2016) and the soil has been contained on site in sealed bags ever since. The measured Olsen-P concentration is 12.6 mg L^{-1}, which is classified as category 1 in the Department of Environment, Food and Rural Affairs (DEFRA) UK system (i.e. some response to P fertiliser expected) and has a recommendation of 40 kg of P ha^{-1} of fertilisation to achieve optimal yields (AHDB, 2023). In this work, we will refer to low-STP soil as soil of category 1 and below, as such, our soil will be classified as a low-STP soil. Soil moisture content was initially adjusted to 12.5% and approximately the same mass of wet soil was added to each column (3469 ± 5 g). The columns were then transferred into a growth cabinet with a 16/8 h day/night cycle, 20 °C air temperature and 50% relative humidity. An automatic watering system was setup to deliver 90 mL of deionized water per day (DI; resistivity = 12 MΩ) to each pot and a tray with DI water to a height of about 5 cm placed underneath the columns complementing the irrigation *via* capillary action. Soil nutrients were added weekly as 25 mL of custom made full strength P-free Hoagland's solution (Hoagland and Arnon, 1950) per pot and additional N and K were supplied once after shoot emergence as NH_4NO_3 at a rate of 62 kg (N) ha^{-1} and KCl at a rate of 50 kg (K) ha^{-1}, respectively. Phosphorus was supplied as triple super phosphate (TSP) granules at 80 kg (P_2O_5) ha^{-1},

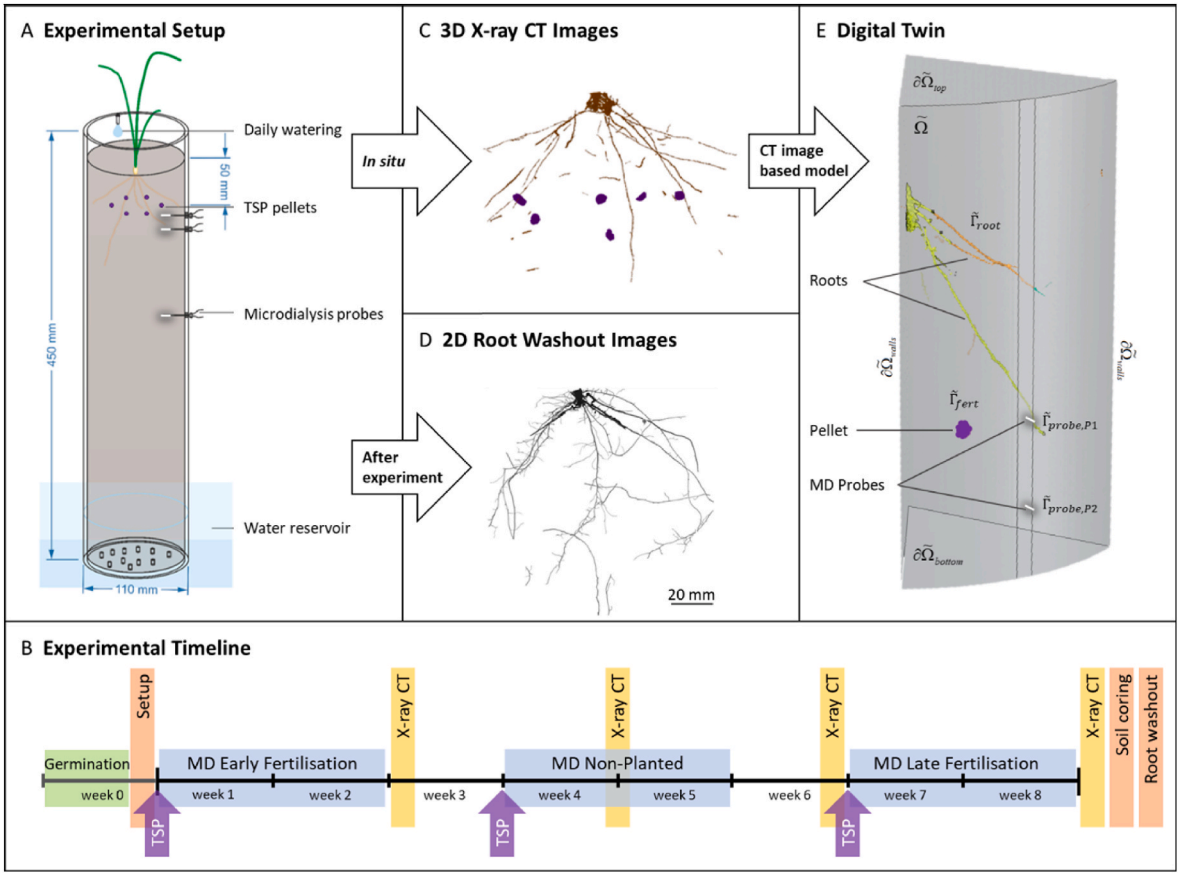

Fig. 1. Study overview. (A) Illustration of the experimental set up consisting of growing wheat plant in a soil column. Each soil column was equipped with three microdialysis probes at different depths. The system was watered daily and supplied with a water reservoir at the bottom. Six TSP fertiliser granules were placed 50 mm below the surface. (B) A diagrammatic schedule of the experiment illustrates the times for the varying treatments (early, non-planted, and late). (C) XCT images were taken every 2 weeks throughout the experiment to monitor plant development and quantify the exact location of the fertiliser granules, roots, and probes in the field of view. (D) Root washout images were taken after the experiment finished, to quantify the number of fine roots that were undetected by the XCT images. (E) XCT images were used to generate domains and explicit boundaries for an image based model, which acts as a 'digital twin' of the experimental system. The digital twins' volume makes up the model domain ($\tilde{\Omega}$) representing homogenous soil, where the artificial walls are denoted by $\partial\tilde{\Omega}_{walls}$, the top is denoted by $\partial\tilde{\Omega}_{top}$, and the bottom is denoted by $\partial\tilde{\Omega}_{bottom}$. The plants, fertiliser granule, and micro-dialysis probes make up internal boundaries and are labelled $\tilde{\Gamma}_{root}$, $\tilde{\Gamma}_{fert}$, $\tilde{\Gamma}_{probe,P1}$, and $\tilde{\Gamma}_{probe,P2}$ respectively. Only one sixth of the imaged volume was used for image based modelling due to computational limitations.

by adding six granules per tube (average mass of the single granule 35 ± 2 mg) at 5 cm depth, 2.5 cm from the pipe walls to avoid preferential water flow patterns, and equidistant from each other (Fig. 1A). Spring wheat seeds were germinated on damp paper for a week and then transferred into soil sowing three seeds per pot. After one week from sowing, pots were thinned and only the most vigorous seedling was kept in each pot.

Three pots were set up for each of the following treatments: an "early fertilisation" treatment where TSP granules were added 1 week after planting, a "late fertilisation" treatment where TSP granules were added 6 weeks after planting (when the roots are expected to have already reached the depth of the granules (Ahmed et al., 2016)), a "non planted" treatment where TSP granules were applied, but no plant was included, and a "blank" treatment where a plant was grown, but no fertiliser was added. A total of 12 pots were setup.

The overview of the experimental setup and design is outlined in Fig. 1A while a timeline of the experiment is shown in Fig. 1B. Wheat plants were sowed into each "early fertilisation", "late fertilisation" and "blank" treatments with replicates; total of 9 plant samples. Six TSP fertiliser granules were added to each "early fertilisation", "non planted" and "late fertilisation" treatments, respectively at week 1, week 4 and week 7 after sowing (Fig. 1B). Microdialysis sampling was carried out for 14 days from fertiliser application for a total of 460 dialysate samples. One blank treatment replicate was monitored during all three of the measurement periods with one microdialysis probe placed at 2.5 cm below the depth at which the granules were placed in the fertilised columns (about 50 samples in total). Root imaging was carried out every two weeks by XCT (Fig. 1C), while root washout and 2D imaging was performed at the end of week 8 for all plant samples (Fig. 1D). Before disrupting the soil columns to wash out the root system, a smaller 1.5 cm diameter soil core was extracted and sectioned for subsequent total P quantification at various depths.

2.2. Soil solution microdialysis sampling and analysis

Three CMA 11 metal-free microdialysis probes (4 mm; 6 kDa cut-off; CMA Microdialysis AB, Sweden) were inserted in each tube at 1.0, 2.5 and 11.5 cm depth from the TSP granule layer, respectively for the "early", "late" and "non planted" pots. For blank treatments, one single probe was added to each pot at a depth of 2.5 cm from the virtual granule level, as P diffusion dynamic is not expected in low-STP soil in the absence of a local P source (Petroselli et al., 2021). Indeed, we observed that the P concentrations in the soil solution detected by the probes in the blank treatment during the three subsequent sets of sampling do not show any particular trend associated with P release into or removal from the soil solution during the whole 8 weeks period, with an average value of 0.1 ± 0.05 ppm (Supplementary Material Fig. S1). These results show that sorbed P into soil solids as well as microbial activity and water flow due to watering from the top of the soil column are negligible in the undisturbed experimental system.

The probes were aligned below one of the granules in order to maximize detection. Probes were perfused with MilliQ water (18 MΩ) at a rate of 3.3 μl min^{-1} (McKay Fletcher et al., 2019; Petroselli et al., 2021) using a PHD 2000 Programmable Syringe Pump (Harvard Apparatus, UK). Sampling time was set to 2 h for the first four samples and 12 h for the rest of the experiment. The obtained dialysate samples were stored in the fridge at +4 °C until analysis in airtight containers. Prior to quantification, dialysate samples were spiked with internal standard elements (Be, In and Re) in a 3% HNO_3 solution to account for matrix drift correction. Quantitative elemental analysis was performed by means of Inductively Coupled Plasma Mass Spectrometry (ICP-MS) at the University of Southampton National Oceanography Centre. A single quadrupole XSeries2 (Thermo-Scientific) was used and seven custom calibration standards were prepared from single element certified standards (Inorganic Ventures TM).

Raw microdialysis data reflects diffusion rate into the probe not soil solution concentration directly. Therefore, dialysate concentrations were converted into soil solution concentrations using a correction factor measured in a previous study (Petroselli et al., 2021) which compared a direct (suction cup) sampling method with microdialysis sampling for the same soil solution concentrations.

Due to the characteristics of the sampling and analysis methods, all presented data of P in dialysates refer to elemental P quantification in samples obtained by passive diffusion of small solute molecules from the soil solution into the dialysis solution. The sampled P compound speciation is beyond the scope of the present paper, however, due to the probe physical features (6 kDa cut-off), we can exclude the sampling of larger molecules (such as DNA), microbes and hydrophobic molecules. We will therefore be referring to P concentrations including the contributions from all the P compounds that are compatible with our sampling technique.

2.3. Soil sampling and analysis

Total P concentration in soil was determined at the end of the experiment by means of total acid digestion followed by ICP-MS analysis. Soil was sampled with a 1.5 cm diameter soil corer and the samples were subjected to total acid digestions with a custom $HF/HClO_4$ protocol until total digestion was achieved. The digestion protocol details can be found in the Supplementary Material section 1.1.2. Quantified elements and calibration are analogues to the ones used for the dialysate samples. These results are not further discussed in the paper because they don't show any noteworthy trend or differences between the treatments. However, averaged data are shown in the Supplementary Material Fig. S11.

2.4. X-ray computed tomography

X-ray computed tomography scans were carried out to visualize the growing roots at 2, 4, 6, and 8 weeks after planting (Fig. 1 B and C). The scans detected the precise location of the microdialysis probes and TSP granules in the system and time-resolved location of the growing plant roots. Before scanning, watering was ceased for at least 1 day to enhance contrast.

Scans were carried out using a custom 450/255 kVp Hutch XCT scanner at the μ-VIS X-ray Imaging Centre, University of Southampton, UK. Each scan used 3142 projections, with eight frames per projection and a 134-ms exposure per frame. The energy chosen was 150 kV at 210 μA. The resulting voxel size was 60 μm. These parameters were chosen to provide sufficient contrast to visualize the roots, soil, probes, and fertiliser granule while minimizing the scan time (each scan took approximately 60 min). The voxel size was the smallest possible so that the entire column diameter fitted within the field of view, to give the highest resolution possible. Scans were reconstructed with a filtered back-projection algorithm in CTPro (Nikon Metrology).

2.4.1. Image processing

Roots were segmented from the surrounding soil using a custom workflow, implemented in a combination of the FIJI distribution of ImageJ (Schindelin et al., 2012; Rueden et al., 2017), a free, open-source software package for image processing and analysis, and Dragonfly (ORS, Quebec, Canada), a commercial piece of image processing, analysis, and visualisation software. Segmented root systems were aligned to label roots that emerged at each time point (Fig. S1) The full workflow is described in the Supplementary Material.

Due to imaging constraints, any roots smaller than 60 μm were not visible in the image since this is the size of one voxel, while segmentation will also remove further small roots, at a minimum those below 120 μm in diameter due to a 1 pixel opening step included in the workflow. This means that only primary roots could be segmented. Segmented root systems were spatially registered across time points to allow the emergence time of each part of the root system to be identified (see

Supplementary Material for full details). The granules and microdialysis probe membrane regions were also added to the segmentations based on the XCT images.

For blank treatments where no fertiliser granules were present, a mock granule was added digitally in the images to generate comparative measurements. The mean granule diameter was chosen by randomly selecting a replicate (L3) and measuring the mean granule diameter of all six granules in the image then calculating a mean of means, giving a diameter of 3.8 mm. A sphere with diameter 3.8 mm was drawn onto the image using the 3D segmentation tools in Dragonfly. All were placed with their centroids on a single plane to match as closely as possible the real granules in the fertilised treatments.

2.4.2. Image measurements

To measure the minimum distance between each probe and the nearest P granule, an exact Euclidean distance transform was generated from the granule image. Then, the grey value at the coordinates of the tip of each probe was measured to give the minimum distance to a granule.

2.4.3. XCT root measurements

Segmented root systems were measured using the BoneJ plugin of ImageJ (Doube et al., 2010). Each root system was skeletonised (thinned to a single line of pixels). The root length was then measured by counting the number of white (root skeleton) pixels and converting into mm.

2.4.4. Root washout root measurements

At the end of the experiment, and after soil coring, the roots were washed out of the soil and photographed to investigate the proportion of roots captured by the XCT imaging. Additional samples were also used for this so that n = 4 for all treatments. Roots were removed from the soil by hand, washed gently with running water to remove as much bound soil as possible then rinsed using deionized water (12 MΩ). Roots were then submerged in water to allow roots to spread out and photographed from below using a Panasonic DMC-FZ330 camera (resolution 4000 × 3000 pixels) with approximately 1 pixel = 60 μm. Images were cleaned using a custom image processing workflow in ImageJ as detailed in the Supplementary Material.

Skeletons were generated for each root system using Skeletonise 2D/3D in ImageJ. Additionally, the 'Local Thickness' function in ImageJ was applied to the binary root washout image to determine the radius of each root pixel. Since the XCT imaging approach did not have the resolution to segment and measure the smaller roots, we instead used the root washout light microscopy images to determine experimental root length and root surface area.

The local thickness and skeleton image of the binary root washout image were used to measure root length and surface area. To calculate the total root length of each replicate, we counted the length contribution of each pixel in the skeletonised images. Length between pixels in contact (including diagonals) was calculated *via* Euclidian distance of their central points. To calculate the root surface area we assumed that each pixel of root in the skeleton image was a perfect cylinder with a diameter value associated with the local thickness map. Each pixel in the skeleton then has an associated surface area. The total root surface area was then the sum of all pixel root surface area contributions. Total root length and root surface area was calculated using Python 3.8 (VanRossum and Drake, 2010) after exporting the skeleton and local thickness images from Fiji.

2.5. Plant biomass measurements

Above ground biomass was recorded fresh and after air-drying, while for below ground biomass, the fresh mass could not be determined due to the washing procedure and it was thus weighed after air-drying only. Plant material was freeze-dried, ground and digested prior to ICP-MS analysis. The digestion protocol used in this case involved the use of a MARS6 microwave digestion system (CEM corporation, USA) and a H_2O_2/HNO_3 reagent mixture (details in the SM section 1.1.3). The obtained samples were then analysed by ICP-MS after an appropriate dilution.

3. Theory and calculation

3.1. Digital twin

3.1.1. Summary and aims

An image-based model of P transport in soil was linked to the geometry derived from the XCT scans producing a digital twin of each experimental replicate. The following experimental details were accounted for in the model development: root geometry as measured from XCT scans with roots growing over time to match experimental data, microdialysis sampling time and position, timing and position of fertiliser application. The lowest probe was not visible in the XCT data but was used as a lower boundary condition. Importantly, full mass balance was achieved accounting for both P removed by soil and by the probes. We excluded P coupling to moisture dynamics (no P-advection (Tinker and Nye, 2000)) because of constant moisture conditions ensured by regular watering, and we also neglect the effects of root organic-acid exudation (Demand et al., 2017; McKay Fletcher et al., 2019, 2020). Further details of the model construction are available in the Supplementary Material.

The modelling of P removal from the soil solution required choosing appropriate P-soil interactions (Ruiz et al., 2021). Our experiment does not allow us to disentangle the P removing processes (i.e. sorption, precipitation and microbial activity), therefore we focused on the overall effect of P removal from the soil solution. We compared two different soil P binding models, namely a standard an equilibrium (Buffer Power (Barber, 1995),) and a dynamic (Absorption-Diffusion) description of the P-soil retention. We compared the model results to the experimental microdialysis results to determine which was more suitable for modelling P transport/retention at these spatial and temporal scales.

3.1.2. Model description

We generated an image-based model as a digital twin to aid in our understanding of the physical phenomena evident in the experimental results. We used the XCT scanned geometry of each replicate to generate a finite element mesh used as domains to solve the P models. Due to the high computational cost to run simulations on such detailed domains, it was only possible to simulate a 6th of the domain (*i.e.* $\widetilde{\Omega}$ represents a sixth sector of the full experiment, Fig. 1E), with each sector centred about the location of a micro-dialysis probe in each. $\widetilde{\Omega}$ represents three-dimensional homogenous soil with volumetric water content $\widetilde{\varphi}_l$ [m^3 of liquid m^{-3} of bulk soil] and volumetric soil solid content $\widetilde{\varphi}_s$ [m^3_{solid} m^{-3}_{bulk}]. We first present the full model with first-order kinetics describing P-soil reactions then describe the assumptions required to derive both the Buffer Power (equilibrium) model and the Absorption-Diffusion (dynamic) model.

To quantify the phosphorus dynamics in the microdialysis experiments, we start by describing the transport dynamics of dissolved phosphorus (P) in a bulk soil domain. Let $\widetilde{c}_l$ [mol m^{-3}_{liquid}] represent the concentration of phosphorus compounds in soil solution and $\widetilde{c}_s$ [mol m^{-3}_{solid}] represent the concentration of phosphorus compounds retained by the soil (i.e. removed from the soil solution). We assume P only moves by diffusion in soil pore water and the P-soil reaction is governed by first order kinetics:

$$\varphi_l \frac{\partial \widetilde{c}_l}{\partial \widetilde{t}} = \widetilde{\nabla} \cdot (\varphi_l \widetilde{D} f \widetilde{\nabla} \widetilde{c}_l) - \varphi_l \widetilde{\beta}_1 \widetilde{c}_l + \varphi_s \widetilde{\beta}_2 \widetilde{c}_s, \widetilde{\mathbf{x}} \in \widetilde{\Omega}, \widetilde{t} \geq 0, \quad (1)$$

where $\widetilde{D}$ [m^2_{liquid} s^{-1}] is the diffusivity of solution P in free liquid, f [-] is the geometric pore-space impedance to diffusion, $\widetilde{\beta}_1$ [s^{-1}] is the effective

absorption rate and $\widetilde{\beta}_2$ [s^{-1}] is the desorption rate. We again stress that the effective absorption rate is a general sink term that accounts for sorption, precipitation and microbial activity. We note that P reaches the microdialysis probes on diffusive time scales (demonstrated in results section), thus it suffices to neglect advection even in the presence of daily watering from the top of the soil column. $\widetilde{c}_s$ is assumed to be immobile and is tracked by conservation of mass (see Supplementary Material for details). At the imaged root interface ($\widetilde{\Gamma}_{root}(t)$) the boundary evolves over time in accordance to the XCT imaged roots, and the uptake is modelled based on Michaelis-Menten kinetics (Barber, 1995).

The microdialysis probes sample P *via* diffusion, thus they are included in the simulations as surface boundary sinks ($\widetilde{\Gamma}_{probe,i}(\widetilde{t})$). Since only the two probes closest to the soil surface were imaged using XCT we only include these probes in the model (Fig. 1E). The times that the probe boundaries $\widetilde{\Gamma}_{probe,i}(\widetilde{t})$ are active are in direct accordance with the experimental sampling protocol.

The fertiliser granule is assumed to release a fixed quantity of P at an exponentially decreasing rate. The fertiliser boundary $\widetilde{\Gamma}_{fert}(t)$ is activated at the time of granule deployment, which is different for early and late treatments. No flux conditions are assumed at the top of the domain ($\partial\widetilde{\Omega}_{top}$), where P is not expected to leave, and at the artificial walls ($\partial\widetilde{\Omega}_{\text{walls}}$), given our assumption that any adjacent sectors would be identical in concentration (each would contain a P pellet in the same position). See the Supplementary Materials for all details of the different boundary and initial conditions.

3.1.3. Modelling buffer power and Absorption-Diffusion

Both the Buffer Power (BP) and the Absorption-Diffusion (AD) models can be derived from eq (1) considering two different scaling arguments. The first argument (*i.e.* the Buffer Power argument) assumes that the rates of absorption and dissolution are similar in magnitude (*i.e.*, $\overline{\beta}_1 \sim \overline{\beta}_2$; Barber, 1995) and the reaction rates are much larger than the characteristic timescale so that we can assume the P-soil reactions are instantaneous relative to the diffusion time-scale (see Supplementary Material for more details). This set of assumption leads to the Buffer Power (BP) model (Ruiz et al., 2021):

$$\underset{\text{model},}{\text{Buffer Power (BP)}}\ (b+\varphi_l)\frac{\partial c_l}{\partial t} = \nabla\cdot(\varphi_l D f \nabla c_l), \mathbf{x}\in\boldsymbol{\Omega}. \quad (2)$$

where $b = \frac{\varphi_l\beta_1}{\beta_2}$. While the Buffer Power model is suitable to describe transport of P in larger scale soil systems, preliminary results suggested it may not be able to capture all the features of the experimental within season shorter time and length scale results (see Results section). Therefore, we seek an alternate model that can better capture microdialysis results. As motivation for the alternate approach, we note that the assumption $\overline{\beta}_1 \sim \overline{\beta}_2$ in the buffer power derivation is not valid for soils with high sorption capacity like that used in this experiment. Soils with high sorption capacity are characterised by high buffer powers, ranging from 40-1000 and typically in the hundreds (Barber, 1995). Since $b = \frac{\varphi_l\beta_1}{\beta_2}$ and φ_l will be on the order of 0.1–0.6 and b on the order of 40–1000, it follows that $\overline{\beta}_1 \gg \overline{\beta}_2$. We use this to define the Absorption-Diffusion reduction. For this model, we neglect the smallest terms (*i.e.* $\overline{\beta}_2$). As such, eq (1) reduces to:

$$\underset{\text{model},}{\text{Adsorption} - \text{Diffusion (AD)}}\ \varphi_l\frac{\partial c_l}{\partial t_1} = (\nabla\cdot(\varphi_l D f \nabla c_l)) - \varphi_l\beta_1 c_l, \mathbf{x}\in\boldsymbol{\Omega} \quad (3)$$

In this study, we compare results from the Buffer Power model (BP, eq. (2)) and the Absorption-Diffusion model (AD, eq. (3)) to determine which is most appropriate for modelling our within season experimental system. All the details about the model derivations and the selection of parameters are included in the Supplementary Material in the Modelling methods section.

3.1.4. Data fitting

3.1.4.1. Fitting the Absorption-Diffusion model to the microdialysis experiment. The experimental microdialysis probes passively take up P from the soil solution *via* diffusion across a membrane. This results in a concentration of P in the dialysate due to the flux of P across the probe membrane over the sampling timescale. However, flux of P is influenced by how closely the probe contacts the soil, the local saturation of the soil and other factors which affect the measurement in addition to soil solution concentration. Thus, a set of parameters were determined for each probe to account for the variability in probe diffusion rates, probe soil-water contact and natural soil variability. Each fitting parameter controls particular aspects of the model probe measurement, see Fig. 2A. The geometric impedance factor f controls the speed of diffusion of P from the fertiliser granule towards the probes. This remained fixed across the samples. The absorption rate $\widetilde{\beta}_1$ controls how much P was bound to the soil (i.e. removed from the soil solution; Fig. 2A) and was allowed to vary between tests, although this was in fact consistent for all tests except one. For all of the tests, we fit different values of probe uptake rates $\widetilde{\delta}_i$ for each replicate for the two imaged probes in the event that probes further from the granule had a higher uptake. The parameters that minimised the square sum (over probe and sample time) difference between the model probe uptake and the experimental measurement was deemed the best fit parameters for each replicate, see Supplementary Materials for exact details on the objective function.

3.1.5. Numerical experiments

3.1.5.1. Comparing the buffer power model and Absorption-Diffusion model to the experimental measurements. The suitability of the two models (*i.e.* Absorption-Diffusion and Buffer Power) for describing the experimental system was assessed based on two comparisons. The first comparison was between the probe uptake estimated by the model for each microdialysis probe and the uptake measured by that probe in the experiment. Unlike the Absorption-Diffusion model, preliminary simulations suggested that the Buffer Power model could not characteristically match the experimental probe measurements as the theoretically observed uptake curve morphology was radically different from experimental observations (i.e. Buffer Power model was only able to characterise the rise in concentration but not the fall), thus we did not perform a rigorous data fitting routine for the Buffer Power model. To illustrate this, we show the model probe uptake for the Buffer Power model using two extreme values for buffer power, $b = 1$ and $b = 40$ to demonstrate that no matter what value for b, f, $\widetilde{\delta}_{P1}$ or $\widetilde{\delta}_{P2}$ is chosen, the buffer model will not be able to match the experiential microdialysis probe uptake measurements. Fig. 2 illustrates the characteristic differences between the Absorption-Diffusion model and Buffer Power model, and it highlights the effect each parameter has on the modelled microdialysis probe measurement. The Absorption-Diffusion model can generate a pulse of P measured by the microdialysis probe (Fig. 2A). Increasing the geometric impedance parameter f in the Absorption-Diffusion model, increases the time it takes for the P from the fertiliser granule to reach the probe (Fig. 2A). The absorption rate $\widetilde{\beta}_1$ controls the width (time the pulse lasts for) and the measured concentration of the pulse. Additionally, the absorption rate determines the decay rate of the pulse of P from the fertiliser in the soil solution. The probe uptake rate $\widetilde{\delta}_i$ controls how much P is taken up by the probe and thus the intensity of the peak. However, the probe uptake will saturate when the probe has depleted all locally available P.

Many of the parameters interact similarly in the Buffer Power model as they do in the Absorption-Diffusion model. The geometric impedance factor f controls the speed at which P from the granule reaches the microdialysis probe and $\widetilde{\delta}_i$ controls how much P is taken up by the probe with a maximum amount dependent on locally available P (Fig. 2B).

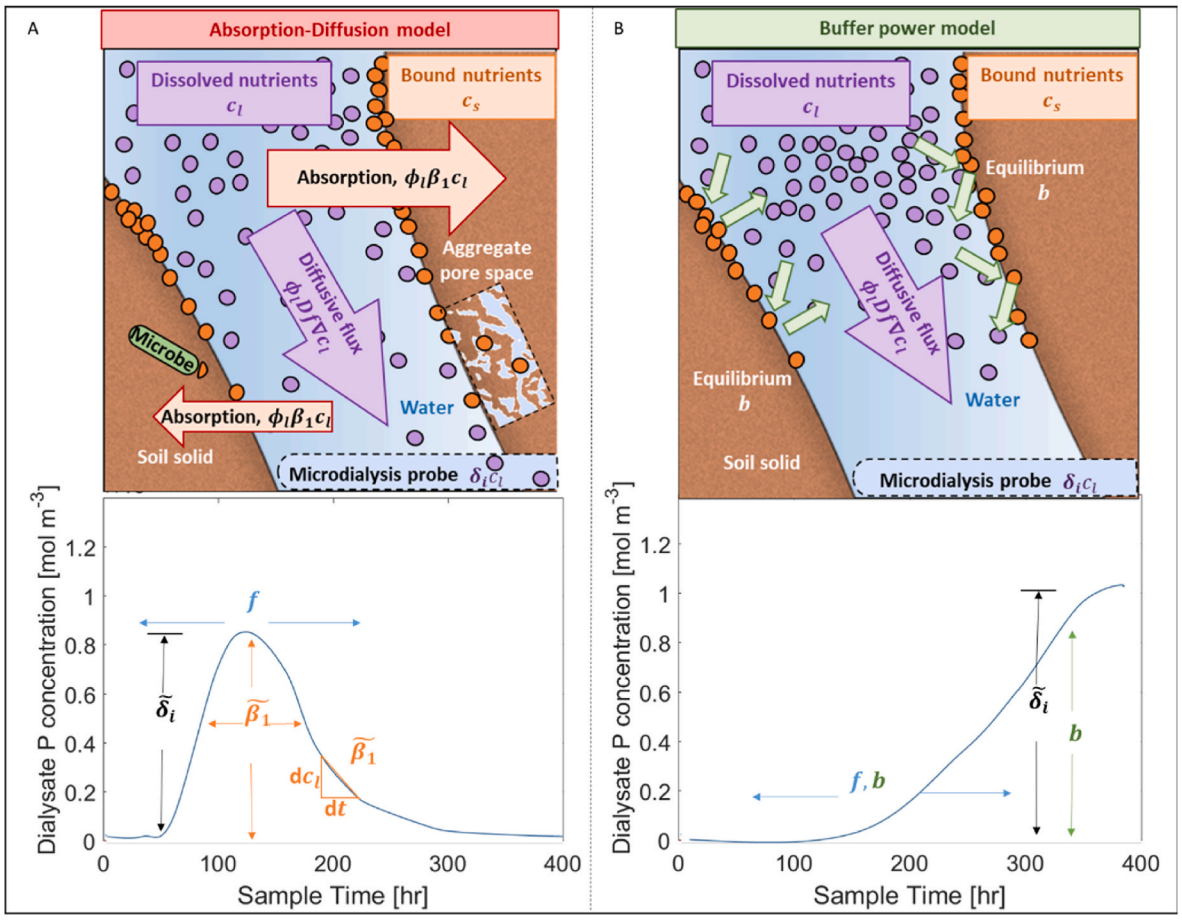

Fig. 2. Visual description of the effect of the parameters on model probe measurement for (A) the Absorption-Diffusion model and (B) the Buffer Power model. (A) The Absorption-Diffusion model considers removal of solute from the soil solution to be the dominating reactive process (e.g. surface binding, aggregate trapped, microbial activity). As such, dialysis probes are expected to sample concentrations of P as they gradually diminish from the solution space based on the absorption rate $\widetilde{\beta}_1$. (B) The Buffer Power model considers that the absorbed and desorbed P are in a constant state of equilibrium based on the ratio between absorption and desorption rates (*i.e.* the buffer power *b*). The buffer power acts to impede rates of transport, thus the probes are expected to sample P at a delayed rate.

Similar to f, the buffer power b limits the speed of diffusion to the probe, (Fig. 2B). For both models there is interplay between the parameters, for example if f increases there is more time for P to be removed from the soil solution, and thus the peak in model microdialysis measurement would be later in time and lower in magnitude. Additionally, the distance of the probe to the fertiliser granule will also affect the model probe measurements.

For the second comparison, each model's root P uptake was compared to the plant total P determination to establish how well they estimated P uptake. The equation for calculating root P uptake in the model can be found in the Supplementary Materials. For the Absorption-Diffusion model, the set of parameters that best fit the microdialysis probe measurements for each replicate were used in this numerical experiment. For the Buffer Power model, we used the Absorption-Diffusion fit uptake parameters and selected $b = 40$ based on previous microdialysis experiments (McKay Fletcher et al., 2019) or as 1 to simulate a low buffering soil. We also compare the model P uptake efficiency of both models to the experimental measurement of P uptake efficiency. In this paper, P uptake efficiency is defined as total plant P uptake per total root surface area and captures how much P the plant takes up per carbon investment in the form of root surface area. Since the XCT imaging did not have the resolution to capture the smallest roots, the root surface area in the models is an underestimate. However, it is likely the roots that were included in the model are in close proximity to those that were missed by the XCT imaging and we expect that the roots in the model are representative of all roots in the experiment's geometric arrangement. Thus, we expect the model will underestimate total P uptake, but be able to capture qualitative differences between treatments. Additionally, we expect the modelled P uptake efficiency to be more in line with the experimental calculation quantitatively because the XCT measured roots were likely to be representative of the location of all roots.

4. Results

4.1. Root measurements

First, we compared the root traits between replicates and treatments to test whether the treatments had resulted in any root responses or differences in plant growth. The mean fresh shoot mass for the Non-fertilised treatment was slightly greater than the Early ($p < 0.05$), but not significantly different from the Late treatment, and there was no difference between the Early and Late treatments (see SM Fig. S2). The root mass did not differ significantly between the treatments, however, based on washout images (Fig. S3), the mean total root length was significantly higher for the Late treatments compared with the Early treatment and the Blank treatment ($p < 0.05$ and < 0.05 respectively) (Fig. S3). Based on the root length measured from the XCT data (Fig. S4), there was no significant difference in mean total root length between the fertilised treatments at 8 weeks (the equivalent time point to the washout experiments), although the mean total root length was consistently the highest through the 8 weeks in the Late treatment.

Looking at the XCT data, the difference in total root length occurred from 2 weeks of growth and persisted throughout the subsequent period (Fig. S4). Although the XCT data underestimates the total root length as the finest roots are not captured, nor are roots that grow beyond the depth of the XCT scan, there is a correlation ($r^2 = 0.458$) between the total lengths measured from the XCT and from the washed-out roots (Fig. S4).

We found no significant differences between any treatments in number of lateral roots with depth or mean lateral root density (Fig. S5), or root length density with depth (Fig. S6). Although we predicted there might be a proliferation of roots near the fertiliser granule when it was added at 8 weeks in the Late treatment, this was not observed in the XCT (Fig. S7). In all but one case, the mean root-soil distance decreased as the roots explored more of the soil through the weeks (Fig. S8), but the roots did not explore the soil to differing extents with respect to the fertiliser treatment (as measured by the mean root-soil distance measure) (Fig. S8).

4.2. Microdialysis

Microdialysis sampling was carried out for all replicates of Early Fertilisation, Late Fertilisation and Non-planted treatments for the two

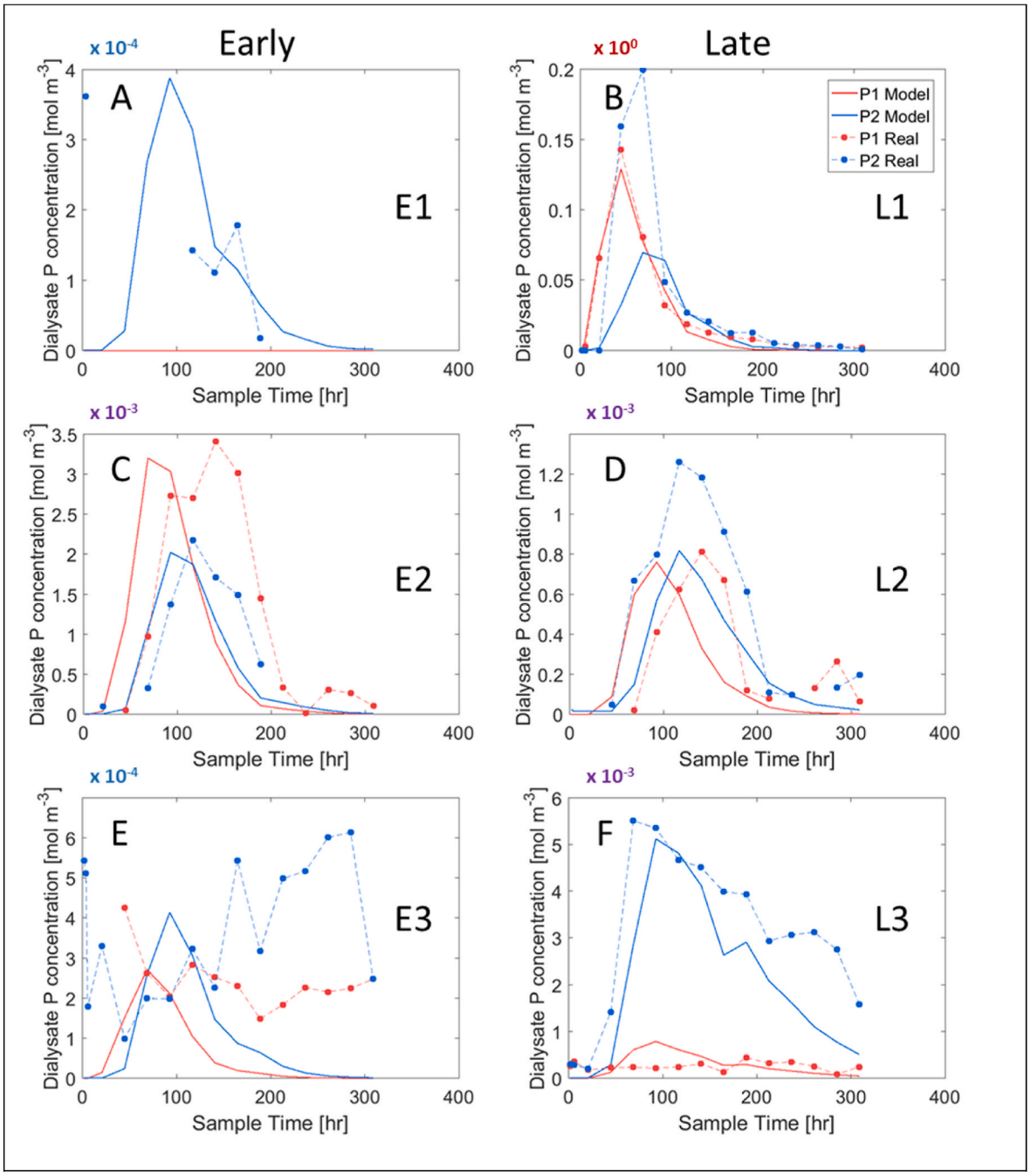

Fig. 3. Phosphorus concentration in the soil solution is reported in function of sample time. Microdialysis experimental results (dots + dashed lines) and Absorption-Diffusion digital twins (solid lines) for Early fertilisation (E1, E2, E3) and Late fertilisation (L1, L2, L3) treatments replicates. Red lines refer to the probe closest to the granule (P1) while blue lines represent the middle probe (P2). Refer to Table 1 for probes-granule distances and to Table 2 for the associated model parameters. Please note that the panels show different scales on the y-axis (blue 10^{-4}, purple 10^{-3}, and red 10^{0}), linked to the variability of the data. This allowed us to clearly show the trends and the accordance of the experimental data with the model.

weeks following fertiliser application (Fig. S10). Averaged elemental P concentrations in the soil solution were determined by microdialysis sampling for each treatment, and are reported in the Supplementary Material Fig. S10 (first row); P concentrations for each individual replicate of Early and Late fertilisation treatments are shown in Fig. 3 (dots and dashed lines). The common trend detected by most of the probes is consistent with what was expected based on Petroselli et al. (2021). The probes detect a phosphorus concentration pulse in the soil solution, characterised by a rapid rise in P concentrations between 0 and 80 h after fertiliser application, a maximum that was reached between 50 and 160 h after fertilisation and a subsequent decrease to approximately pre-fertiliser concentrations after 6–7 days.

Missing data in Fig. 3 can be attributed to low P concentrations that are below the limit of detection and, in some cases, to probe failure. The latter is not unusual when these fragile devices are used in soil, however, the setup design allowed for access and replacement of the probes during the experiment, limiting this issue to very few sampling points. The difficulty in determining low P concentrations, on the other hand, depends on various factors concerning the use of micro-sampling probes such as (1) the dilution operated by the MD probes on the sample (Petroselli et al., 2021), (2) the small size of the probe compared to the size of the pot that implies that the measurements are representative of a very local environment, (3) detectable concentrations depend very strongly on granules-probe vertical alignment which is also linked to the length of the probe that determines how far the probe can penetrate into the soil considering that it needs to be accessible from the outside of the tube. These issues may be linked to the probe positioning and alignment which, together with the limited control on the probe's incline at insertion, resulted in a high variability in the data collected from different replicates.

In light of these considerations, the replicates are discussed individually and the exact location of the MD probes' membranes (position and angle) was determined from the XCT scans in order to support the interpretation of the MD results. The obtained pellet-probe distances are reported in Table 1. Intuitively, the highest P concentrations were recorded for the L1 replicate, where the distances between the probes and the granule are the shortest.

The probes' nominal distances from the vertically aligned granule are P1 = 1.0 cm, P2 = 2.5 cm and P3 = 11.5 cm, however, probe's incline and soil compaction after setup can significantly modify the relative distances between the granule and the probes. This has been observed in a few cases where the second probe (P2) detects the P concentration pulse at the same time as the first probe (P1), see Fig. 3 C and D that correspond to E2 and L2. In these two cases, the vertical distance between the two probes is less than 2 cm which is compatible with the span of the pulse observed in the same soil (Petroselli et al., 2021). Additionally, in L1, L2, and L3 (Fig. 3 B, D and F) the maximum concentration recorded by probe P2 is higher than probe P1. In the L3 case, the first probe ended up above the granule (vertical distance −4.9 mm), explaining the very low concentrations and the diffusive trend, in line with what was observed in Petroselli et al. (2021). In the L1 and L2 cases, this effect cannot be attributed to the probe-granule distance as the probes show a correct vertical distancing and a consistent horizontal alignment (Table 1).

The E1 and E3 replicates show P concentrations that are one order of magnitude lower than the other replicates (10^{-4} versus 10^{-3} mol m^{-3}). The missing data points and the high variability in the data are explained by the low concentrations, which often fall below the limit of detection or within the experimental noise range. As the distance of the probes from the granule in these two cases is not dissimilar to the other replicates both vertically and horizontally, we exclude this to be responsible for the low observed concentrations. The anomaly could be therefore attributed to more local effects, such as the presence of air bubbles near the MD membrane that impede the diffusion of solutes towards the probe, the membrane drying which could lead to membrane damage and rupture, observed in the E1 case, or soil heterogeneity. The obvious way to increase the concentration of P in the MD samples is to use a membrane with large surface area/length. However, this would have at least two challenges: (1) longer membrane would be more fragile and hence more easily breakable in the soil and (2) larger membrane would result in larger soil disturbance hence in more other measurement artefacts.

4.3. Modelling results

For the most part, we found that our modified Absorption-Diffusion model was better able to capture the P dynamics in the soil solution than the standard Buffer Power model. Therefore, in this results section we start by comparing the Absorption-Diffusion model to the experimental data before moving onto comparing the two models. Fig. 3 shows the results of the Absorption-Diffusion model (solid lines) alongside the experimental results. The model predicts that all probes, apart from P1 in E1, should detect a phosphorus pulse. Moreover, the model predicts that the pulse will always reach the closer probe (P1) before being detected by the second one (P2) even though the experimental data show that in some cases the pulses are detected simultaneously by the two probes (Fig. 3 C and D). Regarding the relative concentrations detected by the two probes, the model correctly captures the main variations due to the probe positioning (e.g. L3, Fig. 3F), however, when the probes are close enough to detect the pulse at the same time (e.g. L2, Fig. 3D), the observed differences in the absolute concentration values lose significance as they might be affected by the pulse timing effect that cannot be captured because it is below the experimental time resolution.

The fitted parameters for the Absorption-Diffusion model for each replicate are reported in Table 2. The geometric impedance factor f (which controlled how long it took for P from the fertiliser granule to reach the probes) varied between 0.13 and 0.3, with most replicates requiring the default value 0.3. The best-fit P-soil absorption rate (i.e. P removal from the soil solution due to multiple processes) $\widetilde{\beta}_1$ was 1.1×10^{-5} s^{-1} for all replicates except L3, where the absorption rate was slightly reduced to capture the longer decay in the P2 probe phosphorus concentration measured in this experimental replicate, Fig. 3F. Although we would expect the soil in all replicates to have the same P chemistry, heterogeneity of the soil can explain this result. The probe uptake rates, $\widetilde{\delta}_{P1}$ and $\widetilde{\delta}_{P2}$ varied the most between replicates to account for the probes with no or low P signals below the detection limit of the analytical method and the counter intuitive replicates where P2 had a higher concentration than P1. The Absorption-Diffusion model could characteristically capture the behaviour of the experimental probe

Table 1
Summary of distances of each microdialysis probe to its nearest fertiliser granule. Each value is calculated from the XCT scan and is in mm. z-distance is the distance to the fertiliser granule along axis in the direction of the column height, a negative z-distance means the probe is above the fertiliser granule. xy-distance is the distance to the fertiliser granule in the plane perpendicular to the height axis. Distance is the 3D Euclidean distance to the fertiliser granule.

	E1		E2		E3		L1		L2		L3	
	P1	P2	P1	P2	P1	P2	P1	P2	P1	P2	P1	P2
z-distance	3.0	18.1	4.1	19.4	7.8	21.9	0.9	14.2	9.9	27.0	−4.9	13.0
xy-distance	14.1	14.7	12.7	12.1	11.8	8.9	7.52	8.8	18.6	18.5	13.6	13.8
Distance	14.4	23.3	13.3	22.9	14.1	23.6	7.58	16.7	21.1	32.7	14.5	18.0

measurements where fertiliser P was detected by the probe, *i.e.* E2, L1, L2 and L3, Fig. 3 B, C, D, F. However, the model could not explain why the P2 probe measured a higher concentration of P, for example L2, Fig. 3D.

Although the Absorption-Diffusion model did not perfectly capture the experimental probe measurements, it could capture characteristic features in the experiment that the Buffer Power model could not. When we used the Buffer Power model with buffer power $b = 40$, the diffusion of P from the granule was too slow and the model probes did not detect it at all (Fig. 4A–B). If the buffer power was chosen as 1, then the P from the fertiliser granule reached the probes as it was not much slowed by chemical impedance, but the model probe measurement increased over time and did not decay like the experimental probe measurements (Fig. 4C–D). The decay in experimental probe P measurements was not likely to be caused by root uptake as we saw the same pattern in the non planted treatments (Fig. S10). As further evidence that the roots cannot explain the decline in probe P uptake we increased the root uptake by an order of magnitude ($F_p = 3.26 \times 10^{-7}$) in the Buffer Power model to see if this could result in a decay of the probe P flux. Even with enhanced root uptake, the Buffer Power model could not capture the decay in the experimental probe measurements (Fig. 4 E– F).

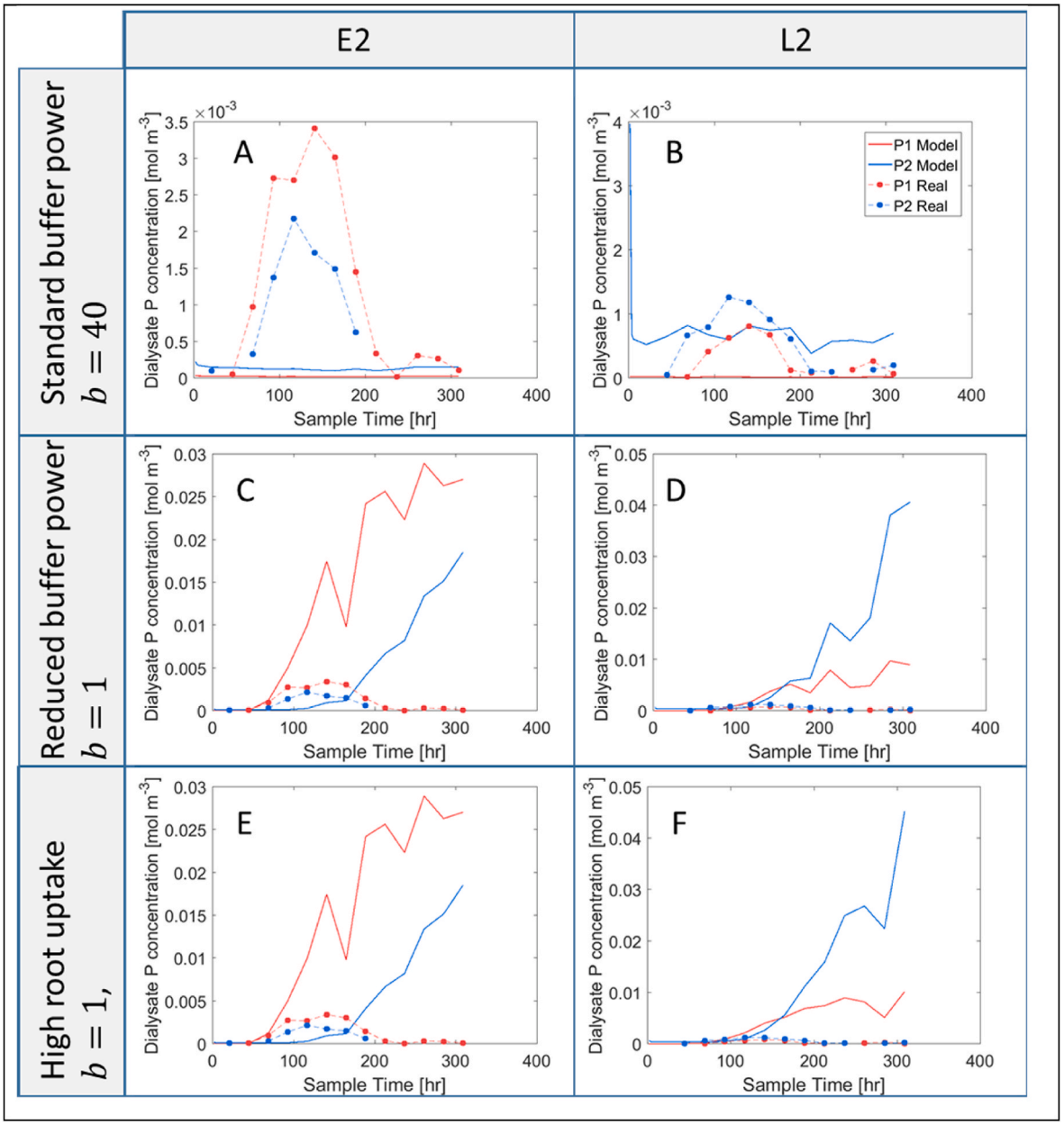

Fig. 4. Experimental microdialysis results (dots + dashed lines) and comparison with Buffer Power model (solid lines) for two example replicates and a range of parameters. The figure demonstrates that the Buffer Power model does not capture the experimental system by showing both a typical and low buffer power selection does not characteristically match the experimental microdialysis results. Each model uses f, $\widetilde{\delta}_{P1}$, and $\widetilde{\delta}_{P2}$ as calculated from the data fitting performed by the Absorption-Diffusion model while b and F_p vary. (A) E2 replicate, Buffer Power model with $b = 40$ and $F_p = 3.26 \times 10^{-8}$ mol m^{-2} s^{-1}. (B) L2 replicate, Buffer Power model with $b = 40$ and $F_p = 3.26 \times 10^{-8}$ mol m^{-2} s^{-1}. (C) E2 replicate, Buffer Power model with $b = 1$ and $F_p = 3.26 \times 10^{-8}$ mol m^{-2} s^{-1}. (D) L2 replicate, Buffer Power model with $b = 1$ and $F_p = 3.26 \times 10^{-8}$ mol m^{-2} s^{-1}. (E) E2 replicate, Buffer Power model with $b = 1$ and $F_p = 3.26 \times 10^{-7}$ mol m^{-2} s^{-1}. (F) L2 replicate, Buffer Power model with $b = 1$ and $F_p = 3.26 \times 10^{-7}$ mol m^{-2} s^{-1}.

4.4. Root uptake

In order to convert soil solution P concentrations to a biologically meaningful measurement, P uptake by the plants was measured both experimentally and numerically. Total elemental P concentrations were determined after total digestion of the plant biomass and are shown in Table 3. There was no significant difference in mean total P uptake between both fertilised treatments and un-fertilised (blank) treatment (two-sided student's t-test, $p > 0.05$). When considering above and below ground material separately the mean P concentrations of both early and late fertilised treatments are slightly higher than those of the blank, though not significantly. There was no significant difference in P uptake efficiency (total P uptake per unit root surface area) between the early, late and blank fertilisation treatments ($p > 0.05$).

To demonstrate the importance of accurately capturing the temporal availability of P from a fertiliser granule, the predicted root uptake dynamics for the two models are shown in Fig. 5. The Absorption-Diffusion model predicted P concentration in the soil solution, thus readily available for root uptake, was only briefly enhanced by the fertiliser granule for approximately $8-13$ days, Fig. 5A. The time (relative to planting) at which P uptake enhancement could happen is dependent on when the fertiliser was added and the time it takes for the P from the granule to dissolve and diffuse to the roots. In the early treatments the granule was added one week after planting and its effect on plant uptake is noticeable almost instantaneously, however, P uptake rate does not reach a peak until approximately 12 days after planting (*i.e.* 5 days after the addition of the fertiliser) Fig. 5A. The enhanced P uptake was only brief and P uptake returned to its pre-fertiliser levels over 10 days. A similar trend can be observed for the late fertilisation replicates where the fertiliser granule was added 49 days after planting, Fig. 5A. In the late fertilisation replicates, the roots had more time to grow, hence we expected the roots to have more chance of taking up the P from the granule before it gets removed from the soil solution. However, this does not seem to be the case, as the root uptake in the late fertilisation is comparable to that of the early treatments (Fig. 5A).

The Buffer Power model ($b = 40$) predicts a characteristically different root P uptake dynamics (Fig. 5B). In the early treatments, we can see a boost in P uptake as soon as the fertiliser is added to the soil at day 7. Unlike the Absorption-Diffusion model, P uptake rate continues to grow in the Buffer Power model as more P from the granule diffuses to the roots (Fig. 5B). The initial peak in root uptake before the fertiliser has been added is due to the roots absorbing the P initially in soil, then the P adjacent to the roots becoming depleted due to slow diffusion resulting in a reduction in root uptake (Fig. 5B).

Fig. 6A shows the total P uptake for the Absorption-Diffusion (in red) and buffer power (in green) models, and the experimentally measured values (in grey). There was no significant difference between the treatments for the Absorption-Diffusion model. For the Buffer Power model, the early replicates have a significantly greater P uptake than the late replicates (one-sided students t-test, $p < 0.05$; Fig. 6A) which is inconsistent with the experimental conclusions (Fig. 6A).

Root P uptake efficiency (RUE) for both models and the experimental measurements is shown in Fig. 6B. The root surface area in the experimental measurements was calculated using the root washout images while the models used the surface area extracted from the XCT scans. The mean of the early experimental root uptake efficiency is not significantly different from the late, (one-sided students t-test, $p > 0.05$, Fig. 6B). The Absorption-Diffusion model correctly predicts no significant difference in uptake efficiency between the early and late treatments while the buffer model predicts a significant difference between early and late treatments with the early P uptake efficiency significantly higher than the late (one-sided students t-test, $p < 0.05$), Fig. 6B, which is inconsistent with the experimental measurement.

Table 2
Parameters in the Absorption-Diffusion model that best matched the microdialysis results. f is soil geometric impedance, $\widetilde{\beta}_1$ is the effective adsorption rate of P, and $\widetilde{\delta}_{Pi}$ are the probe P uptake rates.

Replicate	f	$\widetilde{\beta}_1$ [s^{-1}]	$\widetilde{\delta}_{P1}$ [ms^{-1}]	$\widetilde{\delta}_{P2}$ [ms^{-1}]
E1	0.3	1.1×10^{-5}	0	1×10^{-8}
E2	0.13	1.1×10^{-5}	2×10^{-8}	2×10^{-7}
E3	0.3	1.1×10^{-5}	5×10^{-10}	2×10^{-8}
L1	0.3	1.1×10^{-5}	2.94×10^{-8}	1.47×10^{-5}
L2	0.3	1.1×10^{-5}	1.5×10^{-8}	5×10^{-5}
L3	0.188	4×10^{-6}	2×10^{-9}	3×10^{-8}

Table 3
Mean total P plant uptake and uptake efficiency as calculated from plant digestions at the end of the experiment. Above and below ground P concentration are the concentration in ppm in the above and below ground tissues. Total P is calculated as the sum of mean P concentration in the aboveground and belowground multiplied by their respective mass. P uptake efficiency is calculated as the total P divided by the replicates root surface area as calculated by the light microscopy images. Values show mean ± standard deviation. Different lettered superscripts indicate significant differences as calculated from a two-sided student's t-test.

	Early	Late	Blank
Above ground P concentration (ppm)	$7.8 \times 10^{-3} \pm 3 \times 10^{-2}$	$7.6 \times 10^{-3} \pm 3 \times 10^{-2}$	$6.3 \times 10^{-3} \pm 9 \times 10^{-2}$
Below ground P concentration (ppm)	$5.6 \times 10^{-3} \pm 1 \times 10^{-3}$	$5.4 \times 10^{-3} \pm 6 \times 10^{-2}$	$4.1 \times 10^{-3} \pm 7 \times 10^{-2}$
Total P uptake [mol]	$6.2 \times 10^{-5} \pm 2 \times 10^{-6a}$	$7.3 \times 10^{-5} \pm 7 \times 10^{-6a}$	$6.87 \times 10^{-5} \pm 1 \times 10^{-5a}$
P-uptake efficiency [mol m^{-2}]	$0.018 \pm 3 \times 10^{-3b}$	$0.014 \pm 3 \times 10^{-3b}$	$0.017 \pm 1 \times 10^{-3b}$

5. Discussion

In this study, we investigated the effects of different fertilisation regimes on soil solution P dynamics, plant root structure and growth, and we compared two different models to determine the most adequate to capture the observed dynamics. As seen in some previous studies, adding P fertiliser did not necessarily increase the growth of either the roots or shoots of the plants (Valkama et al., 2011; Macintosh et al., 2019). Here, we also did not find any increase in growth or proliferation of laterals close to the fertiliser granules, despite the use of low-STP soil and the fact that plant roots are known to proliferate in areas of locally high-STP. Not observing effects of the P treatment on plant growth could have multiple concurring causes: (i) added P is removed too quickly from the soil solution to be readily available to the plants; (ii) the plants grew using P reserves in the seed and did not grow long enough to reach the stage when they need to forage P from the surrounding soil; (iii) the alignment between the granules and the growing roots was not optimal to ensure P uptake in the narrow availability time window; (iv) plant growth was hindered by excessive soil moisture that was observed at the end of the experiment. In order to dynamically resolve the evolution of P concentration in the soil solution, we deployed microdialysis probes at various depths of our experimental soil column. Microdialysis results suggest that P is quickly released from the fertiliser granule to the soil solution (no chemical impedance) but is also quickly removed from solution in this low-STP soil (Fig. 3), thus there is only a small time window when the added P from the granule is directly available to the plant roots in the soil solution. Matching this window with plant's needs can become important for precision agriculture practices. The microdialysis probes only detected P from the fertiliser in the soil solution for at most 8 days (Fig. 3C), however, subsequent modelling suggests plants can only access the high concentrations of P in the soil solution for approximately 10 days starting straight after fertilisation (Fig. 5A). This is due to the distribution of roots around the granule, which has to compete against the dynamic removal of P from the soil solution due to multiple processes such as sorption, precipitation and microbial activity.

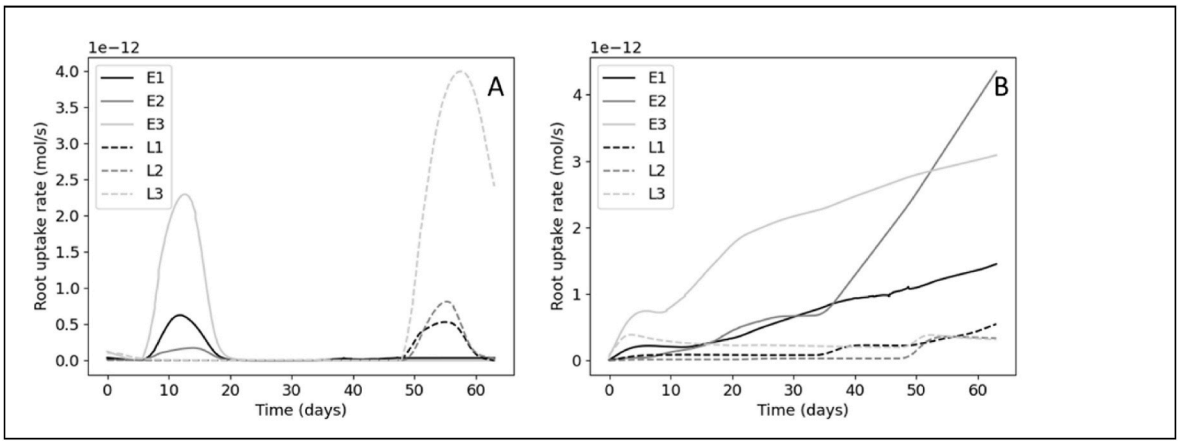

Fig. 5. Comparison of modelled root uptake rates. Time in these plots are relative to planting date. (A) The root uptake rates as predicted by the Absorption-Diffusion model. Each replicate uses the parameters of best fit. (B) The root uptake rates as predicted by the Buffer Power model. Each model uses parameters f, $\widetilde{\delta}_{P1}$ *and* $\widetilde{\delta}_{P2}$ as calculated from the data fitting performed by the Absorption-Diffusion model and the buffer power $b = 40$.

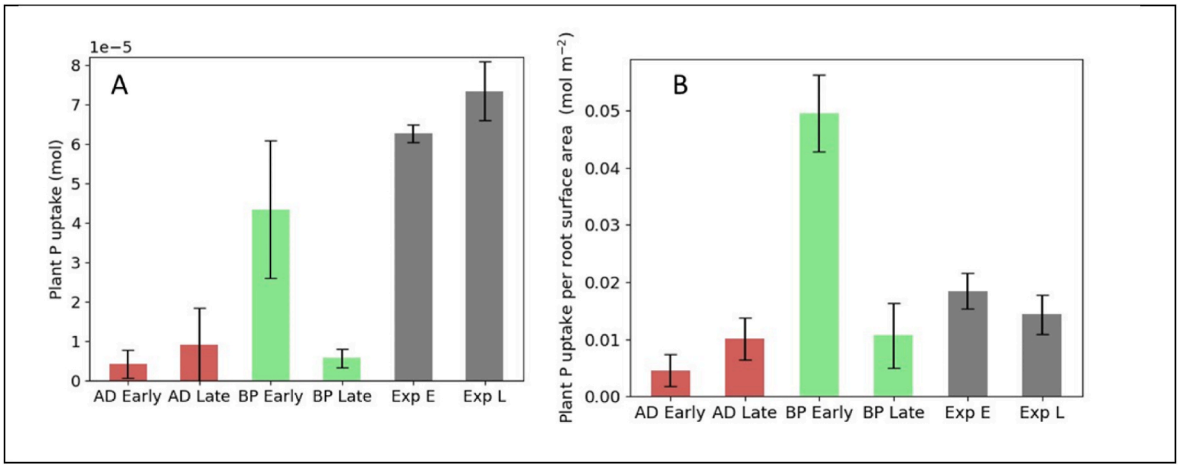

Fig. 6. Mean total root uptake (A) and P uptake efficiency (B) of both models and the experimental measurement over early and late treatments. AD stands for Absorption-Diffusion model, BP stands for Buffer Power model, Exp stands for experimental value, E stands for early replicates and L stands for late replicates. Error bars show standard deviation. For the Absorption-Diffusion model, each replicate uses the parameters of best fit. For the Buffer Power model, each model uses parameters f, $\widetilde{\delta}_{P1}$ *and* $\widetilde{\delta}_{P2}$ as calculated from the data fitting performed by the Absorption-Diffusion model and the buffer power is chosen $b = 40$. (A)Mean total root uptake. (B) Mean P uptake efficiency (Total P uptake per root surface area).

Over the short time-scale of the experiment P removed from the soil solution was not resolubilised, however, we expect the soil-retained P acts as 'Legacy-P' and can improve crop uptake in subsequent growing season (i.e. legacy P (Barrow, 1980)).

Data from the microdialysis measurements provided evidence for the need of a dynamic model capable of capturing the transport and retaining of P in a low-STP soil. This was demonstrated with an Absorption-Diffusion model, however, like all models, it is a simplification of a full kinetic processes that cannot be observed with current technology. Although the model performed characteristically similar to the measured results, there were certain features that could not be resolved by Absorption-Diffusion model. Most notable was that in some cases the middle probe (P2) detected the pulse of P from the granule earlier (E2, L2 and L3) and in higher quantities (L1, L2 and L3) than the probe closest to the granule (Fig. 3). It was unlikely this was due to the variation of the distances between the probes and the granules, as shown in. These counter intuitive results could be explained by the probe uptake rate being affected by local environmental conditions, or possibly, P moving by gravitational effects. It is possible that heavier P particles sink past the first probe and dissolve in proximity of the P2 probe (Petroselli et al., 2021). We expect that this effect is likely to be small as the soil is tortuous, and a large P particle is unlikely to sink far from the fertiliser granule. Root exudation could generate locally enhanced zones of organic acid and low pH, which can act to mobilise soil solid sorbed P (McKay Fletcher et al., 2020). Alternatively, root mucilage could also play a role in reducing effective diffusivity in the soil pore space (Zarebanadkouki et al., 2019). These features are not currently included in the model separately (they are included as a net effect), but it seems at least one of these mechanisms plays a role in P transport from a fertiliser granule and should be investigated in future studies.

However, the first improvements to the model should be the inclusion of the full first-order kinetics (Barber, 1995) or the kinetic Langmuir reaction equation (Van de Weerd et al., 1999; Ruiz et al., 2021; Schnepf et al., 2012). It is important to note that like the Buffer Power model, a Langmuir isotherm (Barber, 1995) would not be able to capture the features seen in the microdialysis results. A Langmuir isotherm diffusion model is a concentration dependent diffusion, with buffer power decreasing as concentration increases. Thus, it would predict microdilayisis probe uptake to be somewhere between the $b = 1$ and $b = 40$ (see Fig. 4) for the Buffer Power model and not be able to capture the decay observed using the experimental microdialysis probes (Fig. 4). In the current study, it was not possible to include full first-order kinetics (i.

e. dynamics associated with desorption of P from the soil/minerals into solution) due to the size and complexity of the domain needed to include root structure; first-order kinetics requires the solution of the retained P equation, which requires additional memory, and was thus not feasible with our computing systems. However, we can conclude that full soil-P dynamics, be it Absorption-Diffusion, first order kinetics or non-linear kinetics like the Langmuir reactions, are required to direct experimental observation of the P dissolution and transport from a fertiliser granule.

Any shortcomings of the Absorption-Diffusion model were also present in equilibrium reaction model exemplified by the Buffer Power model here. The Buffer Power model was not satisfactory for describing the experimental data. For a buffer power used to describe relatively mobile P in soils ($b = 40$), we found that the fertiliser P pulse was impeded so much that it never reached the probes (Fig. 4 A and B). We reduced the buffer power to low values for P, which essentially emulates the situation where all binding sites are occupied (*i.e.* high-STP soil and an extreme case of the Langmuir isotherm model). We found that the pulse makes it to the probes. This resulted in a rise in the probe uptake with no decay (Fig. 4 C and D), which was inconsistent with the data. It was possible that the decay in the experimental measurements was due to root uptake rather soil retaining. This is rejected due to similar results in the non-planted treatment (see SM Fig. S2). Additionally, we increased the uptake by an order of magnitude, which likely breaks the kinetic limitations of the plant P uptake (Barber, 1995). Despite this, the model was still not capable of reproducing the measurements (Fig. 4 E and F). We note that in the previous study, we also found a similar decay behaviour within our experiments, which did not include plant roots (Petroselli et al., 2021). It was clear that no combination of buffer power, geometric impedance and probe uptake rates could achieve the required decay in model probe concentration in the Buffer Power model or any equilibrium reaction model. This result sheds light on some of the details of short-term processes that are often neglected by long term and larger scale models and observation. We note that the soil conditions in this study were low-STP (Olsen P = 12.6 mg L^{-1}) (AHDB, 2023) and that this soil has a high sorption capacity. We attribute the poor performance of the Buffer Power model to reliance on the assumption that the reaction rates are much faster than the diffusion timescale in its derivation (Barber, 1995; Roose et al., 2001), and also note that the Langmuir isotherm diffusion model relies on this same assumption (Van de Weerd et al., 1999; Ruiz et al., 2021). Since the buffer power for soils typically ranges from 40 to 1000, the absorption rate is orders of magnitude bigger than the desorption rate. In this study, we demonstrated that the time scale for absorption was on the same order as the diffusion timescale, which are both much more rapid than the dissolution timescale. Therefore, we did not find that reaction equilibration was a suitable model for describing this experimental system.

We monitored the qualitative behaviour of root uptake in both models. The modelled plant uptake simulated by the Absorption-Diffusion model demonstrates that most of the P is quickly removed from the soil solution so only directly accessible to the plant for a brief period of time (Fig. 5A). By contrast, root uptake in the Buffer Power model remains constant until the fertiliser pulse reaches the rooting zone. Then, in the early fertilisation scenario, the Buffer Power model exhibits an acceleration in the root uptake (Fig. 5B). This acceleration is caused by roots growing into P rich regions or P from the fertiliser granule reaching further the roots. The late replicates with the Buffer Power model did not achieve as high root uptake rates as the early replicates due to experimental cut-off times prior to high P concentrations from the granule reaching the roots. It is worth highlighting that this is a consequence of the time scale of the experiment.

We used the time integrated modelled root P uptake to compare the model results to the total P in the experiments for the early and the late fertiliser application tests. For the early and late fertilisation experiments, there were no significant differences between the total P content in the two treatments (Fig. 6A), however, the mean total P uptake in the late experiments was higher than in the early ones. The experimental total P uptake was generally higher in magnitude by comparison to the simulation results. Additionally, there was no significant difference in total P uptake between the early, late, and no fertiliser experiments, suggesting P fertilisation could only marginally increase P uptake. Differences for the results using the Absorption-Diffusion model, like the experimental results, were not significant. However, the Absorption-Diffusion P uptake was lower in magnitude than the experimentally measured values. By contrast to the Absorption-Diffusion model and the experimental data, the Buffer Power model predicts early fertilisation would result in significantly more total P uptake than the late. This would also imply that legacy-P would be lower for early fertilisation.

The Buffer Power model produced the incorrect conclusion regarding early and late fertilisation. The no fertiliser control experiment alludes to the fact that the plants were unlikely to acquire significant quantities of P from the fertiliser in the first 8 weeks from sowing and much of the measured total P was likely already in the seed and soil from the beginning. The simulations only took into account P taken up from the soil or fertiliser, which might explain why the Absorption-Diffusion model underestimates the P by comparison to the experiments. It is also worth noting that the under-prediction is also likely due to the model missing fine roots during segmentation or because the sixth of the pot was not representative of the entire root system.

To try and account for the underrepresented roots, we compared the root uptake efficiency between the three, *i.e.* experimental results, the Absorption-Diffusion model, and the Buffer Power model (Fig. 6B). Experimentally, the early tests had higher RUE values than the later tests, but the differences were not significant. The Absorption-Diffusion model had slightly higher RUE in the late treatments, but the difference was not significant. Lastly, the Buffer Power model had significantly higher RUE in the early tests. In conclusion, the Buffer Power model appeared to be less in accordance with the experimental data than the Absorption-Diffusion model. While the Absorption-Diffusion model appears to be more representative of the actual experiments, there remain discrepancies between the models and the experimental results in absolute value. These differences could be due to the existence of dissolved P in the soil solution that is below the limits of detection of the analytical method (Petroselli et al., 2021). In this case, the plants in the experiments have access to this low P concentration that is not included in the Absorption-Diffusion model. Other soil P-processes that we did not model which play a role in plant uptake and uptake efficiency could play an important role in P uptake as discussed above. We attribute the poor performance of the equilibrium Buffer Power model in estimating the root uptake in this study to the fact that the soil P was in a state of disequilibrium due the addition of the fertiliser granule and the root uptake. However, agriculture soils are often not in equilibrium (Nair, 2013) and our results demonstrate the importance of considering kinetics.

We can combine these findings together with previous literature to synthesise a general overview of soil P interactions and the resulting implications for crop yield enhancement over one growing season. From literature on soils with more readily available P (*i.e.* high-STP soils, Fig. 7), it appears that applying fertiliser will likely provide minimal enhancement to crop yields that year (Valkama et al., 2011; Macintosh et al., 2019). Under high-STP conditions, once P is removed from the soil solution by the roots, it is replenished by the soil (Rowe et al., 2016). Utilizing this 'legacy P' in high-STP soils is vital for reducing our dependence on rock phosphate and sustainable agriculture (Rowe et al., 2016). Under these conditions, there are diminishing returns on additional P fertilisation in the form of yields (Fig. 7) and P fertilisation comes with risk of leaching and runoff (Fischer et al., 2017; Macintosh et al., 2019). In these scenarios we predict an equilibrium reaction model would be suitable for capturing this scenario since desorption happens faster than in the low-STP case.

Our experiments were conducted on a low-STP soil and we saw negligible increase in plant P uptake with P fertilisation (Table 3) thus

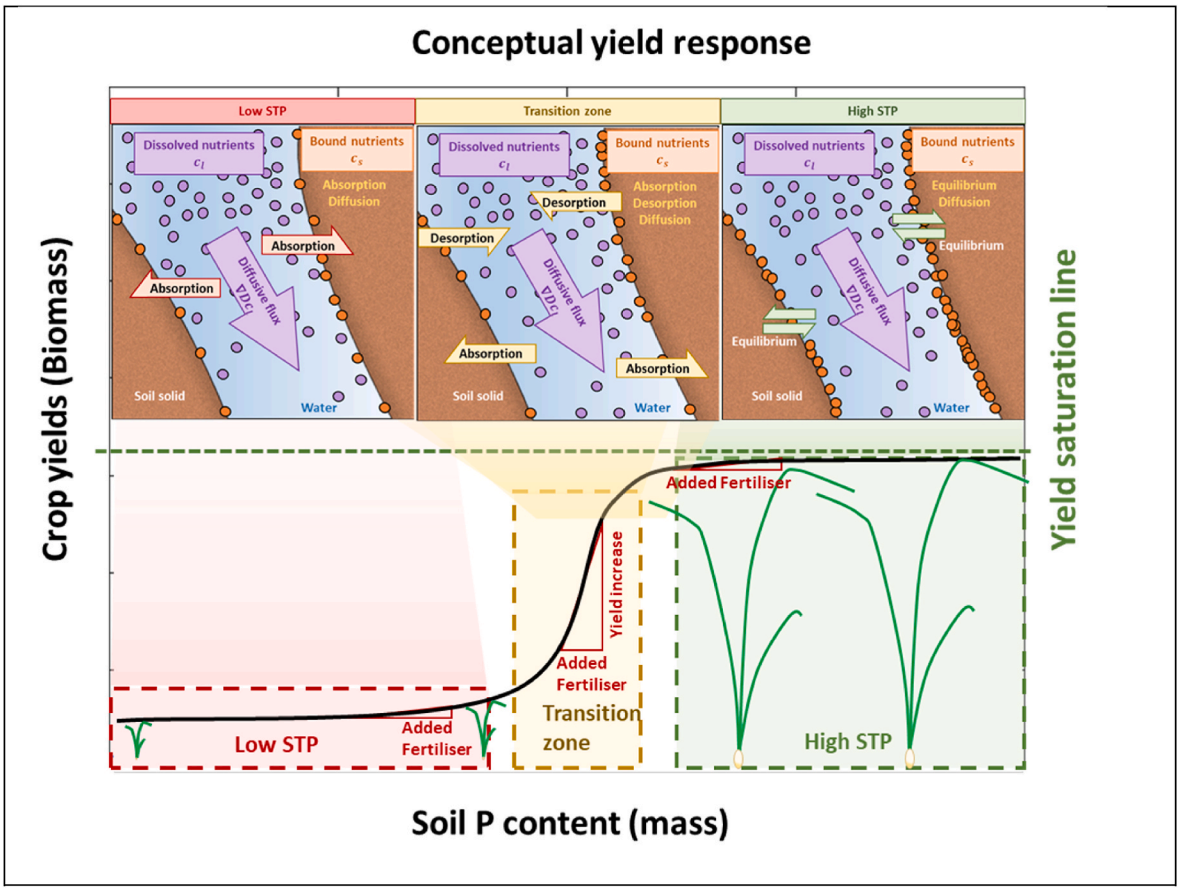

Fig. 7. Conceptual model of crop yields as a function of soil P content. The current study was conducted on a low-STP soil, which required a dynamic Absorption-Diffusion model to characterise the soil P dynamics in a manner that was consistent with the microdialysis measurements. The results suggest that most of the added P fertiliser was rapidly removed from the soil solution before plants could directly access it. Literature studies on high-STP soils appear to demonstrate that there are diminishing returns on added fertilisation, and the systems can be readily modelled considering equilibrium reaction models. There is likely a transition zone where added fertilisation can result in increases in crop yields. We hypothesise that this transition zone would require a full soil type bespoke model that takes into consideration all of the absorption and desorption dynamics.

we deem in these conditions there would be little yield response with this level of fertilisation as conceptually displayed in Fig. 7. There is evidence of poor yield response to P fertilisation in low and medium STP soils, see field trials of (Valkama et al., 2011) for example. Additionally, it is implied with the common use of the Langmuir isotherm where the proportion of plant-available P increases with total P (Barber, 1995). However, with this model one would expect higher P uptake with fertilisation. It is important to note that the experimental conditions only lasted 9 weeks and were not representative of an entire growing season. It could be the case that the crop could utilize the sorbed P over the growing season. However, early P uptake is important for yield (Talboys et al., 2016) and the poor early P uptake in this experiment would have cumulative effect for subsequent yield, regardless of later P utilization. The microdialysis probes determined that the poor P uptake seen in the plant digestions was due to only a brief window (approximately 5–8 days) of enhanced solution P availability (Fig. 3). Modelling suggests that this brief window only lasts for approximately 10 days (Fig. 5). There seems to be two options for improving P uptake and thus yield in low-STP soils with P fertilisation. First, apply large quantities of P to saturate the soil P binding sites and get to the rapidly increasing point on the curve shown in Fig. 7. It is possible this could take a number of years. However, this approach is expensive and carries the risk of nutrient leaching and run-off (Fischer et al., 2017).

Alternatively, precision agriculture techniques (Cisternas et al., 2020) in combination with plant breeding could be used to make the most of the brief window of enhanced P uptake. This might be achieved through a few different avenues. For example, precision placement of the fertiliser to ensure maximal root proximity, or timing the application with rainfall and soil moisture to control the pulse of available P from the fertiliser granule. Results suggest that when sampling the soil for precision agriculture techniques, the brief time-window of P availability in the soil solution should be taken into consideration. Plant traits such as the exudation of organic acids could help the plant solubilise retained P after the initial pulse (Jones, 1998; Gerke et al., 2000). Thus breeding and using high exuding varieties (McGrail et al., 2021) could improve P uptake in the current conditions. To test the role organic acids in P acquisition from a fertiliser granule in these conditions, we recommend using the current experimental setup, but infusing the microdialysis probes with organic acids which exude into the soil while simultaneously sampling soil solution P (Demand et al., 2017; McKay Fletcher et al., 2019).

It appears that when adding P fertiliser granules to a low-STP soil, roots will be in competition with the soil to take up the pulse of solution P from the fertiliser – a feature that is not accounted for when using equilibrium models like the Buffer Power model. Furthermore, neither early nor late fertilisation will make a difference on these time scales. In these conditions it is important to make use of plant strategies for solubilising and harvesting retained P (Wen et al., 2019). From previous literature it is clear adding fertilisers to a high-STP soil will not provide any benefit, as there is likely abundant P for plant use. However, there is likely to be a regime between low-STP and high-STP where there will be a good yield response to fertilisation (Fig. 7), but this would be very soil

type dependent. Within this regime, neither of the models used in this study will likely be adequate for describing the dynamics of the system. To properly estimate the gains in this regime, the full model (eq. (1)) will likely need to be invoked.

Understanding how soil P dynamics in low-STP and high-STP regimes can curb larger scale P deficits through enhancing fertiliser use efficiency, which will aid in larger sustainable practices (Cordell et al., 2009). For example, arable land in the UK makes up over 3×10^6 ha of land. Assuming that there's an accumulation rate of 5.7 kg ha^{-1} yr^{-1} (estimated by the 700 kg ha^{-1} accumulation in the EU since 1900 (Kahiluoto et al., 2021)) and the cost of P fertilisers is at 0.320 EUR kg^{-1} (Mundi, 2022), this means that the UK can be saving over 5 M EUR annually through efficient P allocation. Moreover, identifying the transition zone between low-STP to high-STP soils will also help in planning sensible fertilisation strategies. Finally, future studies will have to identify the nuanced dynamics that take place during the transition between high-STP to low-STP in order to avoid future losses considering the current volatile prices for P (Mundi, 2022).

Acknowledgements and funding statements

The authors would like to acknowledge the μ-VIS X-ray Imaging Centre at the University of Southampton for provision of tomographic imaging facilities, and in particular Dr. Sebastian Rosini and Dr. Kathryn Rankin for their valuable support with the XCT scans. C.P, S.A.R., K.A.W, D.M.F. and T.R. are funded by ERC Consolidator grant 646809 (Data Intensive Modelling of the Rhizosphere Processes). T.R. is also funded by, BBSRC SARIC BB/P004180/1, BBSRC SARISA BB/L025620/1 and EPSRC EP/M020355/1. S.A.R is also funded by BBSRC Discovery Fellowship BB/X010147/1 and Royal Society University Research Fellowship URF\R1\231622. D.M.F: This work was supported by the Rural and Environment Science and Analytical Services Division (SRUC-C5-1).

CRediT authorship contribution statement

C. Petroselli: Writing – original draft, Software, Methodology, Investigation, Formal analysis, Data curation, Conceptualization. **K.A. Williams:** Writing – original draft, Methodology, Investigation, Formal analysis, Data curation. **S.A. Ruiz:** Writing – original draft, Methodology, Investigation, Formal analysis, Data curation, Conceptualization. **D. McKay Fletcher:** Writing – original draft, Software, Investigation, Formal analysis, Data curation. **M.J. Cooper:** Formal analysis. **T. Roose:** Project administration, Methodology, Investigation, Funding acquisition, Formal analysis, Conceptualization, Resources, Supervision, Writing – review & editing.

Declaration of competing interest

The authors declare that they have no known competing financial interests or personal relationships that could have appeared to influence the work reported in this paper.

Data availability

Data will be made available on request.

Appendix A. Supplementary data

Supplementary data to this article can be found online at https://doi.org/10.1016/j.soilbio.2024.109417.

References

AHDB, U., 2023. Nutrient Management Guide (RB209). AHDB Warwickshire, UK.
Ahmed, S., Klassen, T.N., Keyes, S., Daly, M., Jones, D.L., Mavrogordato, M., Sinclair, I., Roose, T., 2016. Imaging the interaction of roots and phosphate fertiliser granules using 4D X-ray tomography. Plant and Soil 401, 125–134.
Barber, S.A., 1995. Soil Nutrient Bioavailability: a Mechanistic Approach. John Wiley & Sons.
Barrow, N., 1974. The slow reactions between soil and anions: 1. Effects of time, temperature, and water content of a soil on the decrease in effectiveness of phosphate for plant growth. Soil Science 118, 380–386.
Barrow, N., 1980. Evaluation and utilization of residual phosphorus in soils. The role of phosphorus in agriculture 333–359.
Barrow, N., 1983. A mechanistic model for describing the sorption and desorption of phosphate by soil. Journal of Soil Science 34, 733–750.
Benbi, D., Gilkes, R., 1987. The movement into soil of P from superphosphate grains and its availability to plants. Fertilizer Research 12, 21–36.
Bolland, M.D., Gilkes, R.J., 1998. The chemistry and agronomic effectiveness of phosphate fertilizers. Journal of Crop Production 1, 139–163.
Buckley, S., Brackin, R., Jämtgård, S., Näsholm, T., Schmidt, S., 2020. Microdialysis in soil environments: current practice and future perspectives. Soil Biology and Biochemistry 143, 107743.
Cisternas, I., Velásquez, I., Caro, A., Rodríguez, A., 2020. Systematic literature review of implementations of precision agriculture. Computers and Electronics in Agriculture 176, 105626.
Condron, L.M., Turner, B.L., Cade-Menun, B.J., 2005. Chemistry and dynamics of soil organic phosphorus. Phosphorus: Agriculture and Environment 46, 87–121.
Cordell, D., Drangert, J.-O., White, S., 2009. The story of phosphorus: global food security and food for thought. Global Environmental Change 19, 292–305.
Cornish, P.S., 2009. Research directions: improving plant uptake of soil phosphorus, and reducing dependency on input of phosphorus fertiliser. Crop & Pasture Science 60, 190–196.
Demand, D., Schack-Kirchner, H., Lang, F., 2017. Assessment of diffusive phosphate supply in soils by microdialysis. Journal of Plant Nutrition and Soil Science 180, 220–230.
Doube, M., Kłosowski, M.M., Arganda-Carreras, I., Cordelières, F.P., Dougherty, R.P., Jackson, J.S., Schmid, B., Hutchinson, J.R., Shefelbine, S.J., 2010. BoneJ: free and extensible bone image analysis in ImageJ. Bone 47, 1076–1079.
Fischer, P., Pöthig, R., Venohr, M., 2017. The degree of phosphorus saturation of agricultural soils in Germany: current and future risk of diffuse P loss and implications for soil P management in Europe. Science of the Total Environment 599, 1130–1139.
Gao, W., Blaser, S.R., Schlüter, S., Shen, J., Vetterlein, D., 2019a. Effect of localised phosphorus application on root growth and soil nutrient dynamics in situ–comparison of maize (Zea mays) and faba bean (Vicia faba) at the seedling stage. Plant and Soil 441, 469–483.
Gao, W., Schlüter, S., Blaser, S.R., Shen, J., Vetterlein, D., 2019b. A shape-based method for automatic and rapid segmentation of roots in soil from X-ray computed tomography images: rootine. Plant and Soil 441, 643–655.
Gerke, J., Beißner, L., Römer, W., 2000. The quantitative effect of chemical phosphate mobilization by carboxylate anions on P uptake by a single root. I. The basic concept and determination of soil parameters. Journal of Plant Nutrition and Soil Science 163, 207–212.
Hammarlund-Udenaes, M., 2017. Microdialysis as an important technique in systems pharmacology—a historical and methodological review. The AAPS Journal 19, 1294–1303.
Hedley, M., McLaughlin, M., 2005. Reactions of phosphate fertilizers and by-products in soils. Phosphorus: Agriculture and Environment 46, 181–252.
Hoagland, D.R., Arnon, D.I., 1950. The water-culture method for growing plants without soil. Circular 347 (32). California agricultural experiment station.
Jones, D.L., 1998. Organic acids in the rhizosphere–a critical review. Plant and Soil 205, 25–44.
Kahiluoto, H., Pickett, K.E., Steffen, W., 2021. Global nutrient equity for people and the planet. Nature Food 2, 857–861.
König, A., Wiesenbauer, J., Gorka, S., Marchand, L., Kitzler, B., Inselsbacher, E., Kaiser, C., 2022. Reverse microdialysis: a window into root exudation hotspots. Soil Biology and Biochemistry 174, 108829.
Macintosh, K.A., Doody, D.G., Withers, P.J., McDowell, R.W., Smith, D.R., Johnson, L.T., Bruulsema, T.W., O'Flaherty, V., McGrath, J.W., 2019. Transforming soil phosphorus fertility management strategies to support the delivery of multiple ecosystem services from agricultural systems. Science of the Total Environment 649, 90–98.
McGrail, R.K., Van Sanford, D.A., McNear Jr., D.H., 2021. Semidwarf winter wheat roots contain fewer organic acids than wild-type varieties under phosphorus stress. Crop Science 61, 3586–3597.
McKay Fletcher, D., Shaw, R., Sánchez-Rodríguez, A., Daly, K., Van Veelen, A., Jones, D., Roose, T., 2019. Quantifying citrate-enhanced phosphate root uptake using microdialysis. Plant and Soil 1–21.
McKay Fletcher, D.M., Ruiz, S., Dias, T., Petroselli, C., Roose, T., 2020. Linking root structure to functionality: the impact of root system architecture on citrate-enhanced phosphate uptake. New Phytologist 227, 376–391.
Mundi, I., 2022. Rock Phosphate Monthly Price–Euro Per Metric Ton.
Nair, K.P., 2013. The buffer power concept and its relevance in African and Asian soils. Advances in Agronomy 121, 447–516.
Nziguheba, G., Zingore, S., Kihara, J., Merckx, R., Njoroge, S., Otinga, A., Vandamme, E., Vanlauwe, B., 2016. Phosphorus in smallholder farming systems of sub-Saharan Africa: implications for agricultural intensification. Nutrient Cycling in Agroecosystems 104, 321–340.

Oburger, E., Jones, D.L., Wenzel, W.W., 2011. Phosphorus saturation and pH differentially regulate the efficiency of organic acid anion-mediated P solubilization mechanisms in soil. Plant and Soil 341, 363–382.
Oburger, E., Kirk, G.J., Wenzel, W.W., Puschenreiter, M., Jones, D.L., 2009. Interactive effects of organic acids in the rhizosphere. Soil Biology and Biochemistry 41, 449–457.
Petroselli, C., Williams, K.A., Ghosh, A., McKay Fletcher, D., Ruiz, S.A., Gerheim Souza Dias, T., Scotson, C.P., Roose, T., 2021. Space and time-resolved monitoring of phosphorus release from a fertilizer pellet and its mobility in soil using microdialysis and X-ray computed tomography. Soil Science Society of America Journal 85, 172–183.
Pierzynski, G.M., McDowell, R.W., Thomas Sims, J., 2005. Chemistry, cycling, and potential movement of inorganic phosphorus in soils. Phosphorus: Agriculture and Environment 46, 51–86.
Roose, T., Fowler, A., Darrah, P., 2001. A mathematical model of plant nutrient uptake. Journal of Mathematical Biology 42, 347–360.
Ros, M.B., Koopmans, G.F., van Groenigen, K.J., Abalos, D., Oenema, O., Vos, H.M., van Groenigen, J.W., 2020. Towards optimal use of phosphorus fertiliser. Scientific Reports 10, 1–8.
Rowe, H., Withers, P.J., Baas, P., Chan, N.I., Doody, D., Holiman, J., Jacobs, B., Li, H., MacDonald, G.K., McDowell, R., 2016. Integrating legacy soil phosphorus into sustainable nutrient management strategies for future food, bioenergy and water security. Nutrient Cycling in Agroecosystems 104, 393–412.
Rueden, C.T., Schindelin, J., Hiner, M.C., DeZonia, B.E., Walter, A.E., Arena, E.T., Eliceiri, K.W., 2017. ImageJ2: ImageJ for the next generation of scientific image data. BMC Bioinformatics 18, 529.
Ruiz, S., Mckay Fletcher, D., Williams, K., Roose, T., 2021. Plant–soil modelling. Annu. Plant Rev. Online 4, 127–198.
Sattari, S., Van Ittersum, M., Giller, K., Zhang, F., Bouwman, A., 2014. Key role of China and its agriculture in global sustainable phosphorus management. Environmental Research Letters 9, 054003.
Sattari, S.Z., Bouwman, A.F., Giller, K.E., van Ittersum, M.K., 2012. Residual Soil Phosphorus as the Missing Piece in the Global Phosphorus Crisis Puzzle, vol. 109. Proceedings of the National Academy of Sciences, pp. 6348–6353.
Schachtman, D.P., Reid, R.J., Ayling, S.M., 1998. Phosphorus uptake by plants: from soil to cell. Plant Physiology 116, 447–453.
Schindelin, J., Arganda-Carreras, I., Frise, E., Kaynig, V., Longair, M., Pietzsch, T., Preibisch, S., Rueden, C., Saalfeld, S., Schmid, B., 2012. Fiji: an open-source platform for biological-image analysis. Nature Methods 9, 676–682.
Schnepf, A., Leitner, D., Klepsch, S., 2012. Modeling phosphorus uptake by a growing and exuding root system. Vadose Zone Journal 11.
Talboys, P.J., Heppell, J., Roose, T., Healey, J.R., Jones, D.L., Withers, P.J., 2016. Struvite: a slow-release fertiliser for sustainable phosphorus management? Plant and Soil 401, 109–123.
Tinker, P.B., Nye, P.H., 2000. Solute Movement in the Rhizosphere. Oxford University Press.
Valkama, E., Uusitalo, R., Turtola, E., 2011. Yield response models to phosphorus application: a research synthesis of Finnish field trials to optimize fertilizer P use of cereals. Nutrient Cycling in Agroecosystems 91, 1–15.
Van de Weerd, H., Van Riemsdijk, W., Leijnse, A., 1999. Modeling the dynamic adsorption/desorption of a NOM mixture: effects of physical and chemical heterogeneity. Environmental Science and Technology 33, 1675–1681.
VanRossum, G., Drake, F.L., 2010. The python Language Reference. Python Software Foundation, Amsterdam, Netherlands.
Wen, Z., Li, H., Shen, Q., Tang, X., Xiong, C., Li, H., Pang, J., Ryan, M.H., Lambers, H., Shen, J., 2019. Tradeoffs among root morphology, exudation and mycorrhizal symbioses for phosphorus-acquisition strategies of 16 crop species. New Phytologist 223, 882–895.
Williams, K., McKay Fletcher, D., Petroselli, C., Ruiz, S., Roose, T., 2022. A 3D image-based modelling approach for understanding spatiotemporal processes in phosphorus fertiliser dissolution, soil buffering and uptake by plant roots. Scientific Reports 12, 1–13.
Zarebanadkouki, M., Fink, T., Benard, P., Banfield, C.C., 2019. Mucilage facilitates nutrient diffusion in the drying rhizosphere. Vadose Zone Journal 18, 1–13.